

NO-A178 895 MAGNETICALLY INSULATED OPENING SWITCH RESEARCH(U) AVCO 1/1
RESEARCH LAB INC EVERETT MA M W MC GEOCH ET AL JAN 87
ARO-21019 3-PH DARC29-84-C-0007

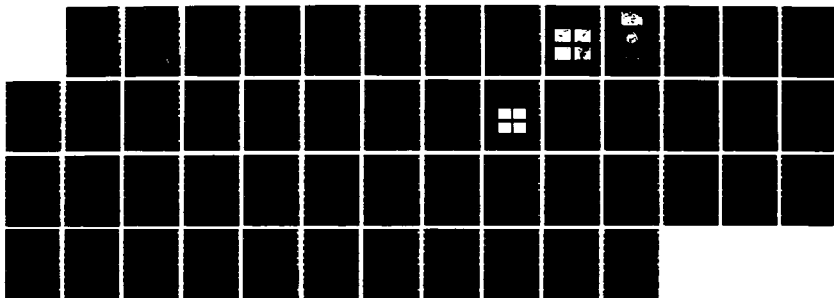
MAGNETICALLY INSULATED OPENING SWITCH RESEARCH(U) AVCO
RESEARCH LAB INC EVERETT MA M W MCGEOCH ET AL JAN 87
ARO-21019 3-PH DAAC29-84-C-0007

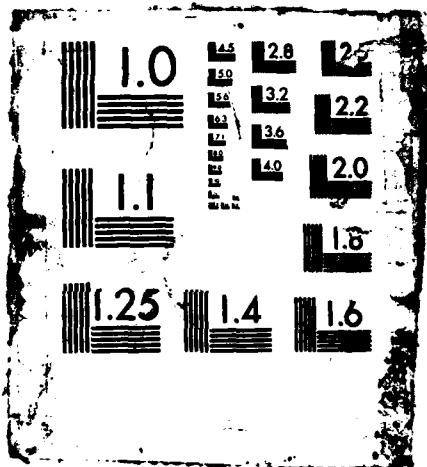
1/1

UNCLASSIFIED

F/G 9/1

NL





1.0

1.1

1.25

1.5
1.6
1.8
2.0
2.2
2.5
2.8
3.2
3.6
4.0

2.8

3.2

3.6

4.0

2.5

2.2

2.0

1.8

1.4

1.6

(2)

AD-A178 895

Magnetically Insulated Opening Switch Research

Final Report

M. W. McGeoch and R. Kraft

January 1987

prepared for

U. S. Army Research Office
P. O. Box 12211
Research Triangle Park, NC 27709

Contract No. DAAC29-84-C-0007

prepared by

Avco Research Laboratory, Inc.
A Subsidiary of Textron, Inc.
2385 Revere Beach Parkway
Everett, Massachusetts 02149

DTIC
ELECTE
S APR 6 1987
A

Approved for Public Release; Distribution Unlimited

87 4 1 327

UNCLASSIFIED

AD-A178895

SECURITY CLASSIFICATION OF THIS PAGE (When Data Entered)

REPORT DOCUMENTATION PAGE		READ INSTRUCTIONS BEFORE COMPLETING FORM
1. REPORT NUMBER ARO 21019-3 PH	2. GOVT ACCESSION NO. N/A	3. RECIPIENT'S CATALOG NUMBER N/A
4. TITLE (and Subtitle) Magnetically Insulated Opening Switch Research		5. TYPE OF REPORT & PERIOD COVERED Final Report June 84-Oct 86
		6. PERFORMING ORG. REPORT NUMBER
7. AUTHOR(s) M.W. McGeoch and R. Kraft		8. CONTRACT OR GRANT NUMBER(s) DAAC 29-84-C-0007
9. PERFORMING ORGANIZATION NAME AND ADDRESS Avco Research Laboratory, Inc. a Subsidiary of Textron, Inc. 2385 Revere Beach Parkway Everett, MA 02149		10. PROGRAM ELEMENT, PROJECT, TASK AREA & WORK UNIT NUMBERS
11. CONTROLLING OFFICE NAME AND ADDRESS U.S. Army Research Office Post Office Box 12211 Research Triangle Park, NC 27709		12. REPORT DATE January 1987
		13. NUMBER OF PAGES
14. MONITORING AGENCY NAME & ADDRESS (if different from Controlling Office)		15. SECURITY CLASS. (of this report) Unclassified
		15a. DECLASSIFICATION/DOWNGRADING SCHEDULE
16. DISTRIBUTION STATEMENT (of this Report) Approved for public release; distribution unlimited.		
17. DISTRIBUTION STATEMENT (of the abstract entered in Block 20, if different from Report) NA		
18. SUPPLEMENTARY NOTES The view, opinions, and/or findings contained in this report are those of the author(s) and should not be construed as an official Department of the Army position, policy, or decision, unless so designated by other documentation.		
19. KEY WORDS (Continue on reverse side if necessary and identify by block number) Magnetic Insulation, Magnetron, Thermionic Diode, Opening Switch, Plasma Waves, <i>Chief</i>		
20. ABSTRACT (Continue on reverse side if necessary and identify by block number) We examine the feasibility of an opening switch concept based on magnetic insulation in a coaxial thermionic diode. It is found that the impedance ratio between 'closed' and 'open' states of the diode is marginal for efficient energy transfer via this type of switch. The open, or insulated state of the diode is characterized by current leakage across the magnetic field which is associated with the presence of plasma waves. This leakage		

DD FORM 1473

JAN 73

EDITION OF 1 NOV 65 IS OBSOLETE

UNCLASSIFIED

SECURITY CLASSIFICATION OF THIS PAGE (When Data Entered)

UNCLASSIFIED

SECURITY CLASSIFICATION OF THIS PAGE(When Data Entered)

can be related to that previously observed in the smooth-anode magnetron. It obeys the relation

$$I = \frac{0.84 \times 10^{-6} \xi A_C V^{3/2}}{d_{\text{eff}}} \exp \left\{ \frac{4015 x_*}{\xi} \right\} \text{ Amps}$$

where A_C is the cathode area, V the anode-cathode voltage, d_{eff} is an effective interelectrode gap (m) and x_* is the thickness of the Brillouin layer in contact with the cathode (m). ξ is a geometrical factor equal to unity in a nearly planar geometry, increasing to 3 as the cathode radius becomes much less than the anode radius. Probe measurements have revealed electrostatic transverse magnetic (TM) waves at frequencies predominantly below the cyclotron frequency with wavelengths equal to $\pi d/n$ where d = diode diameter and $n = 1, 2, 3, \dots$. There is a strong correlation between the amplitude of these waves and the leakage current.

UNCLASSIFIED

SECURITY CLASSIFICATION OF THIS PAGE(When Data Entered)

TABLE OF CONTENTS

<u>Section</u>		<u>Page</u>
	List of Illustrations	v
1.0	INTRODUCTION	1
2.0	EFFICIENCY SCALING OF MAGNETICALLY INSULATED OPENING SWITCH	5
APPENDIX		
1.0	INTRODUCTION	13
2.0	EXPERIMENTAL APPARATUS	15
3.0	DIODE CHARACTERIZATION	21
4.0	LAMINAR FLOW MODEL	27
5.0	WAVE MEASUREMENTS	31
6.0	CORRELATION BETWEEN WAVE AMPLITUDE AND LEAKAGE CURRENT	39
7.0	SUMMARY AND CONCLUSION	27



DTIC	<input checked="" type="checkbox"/>
COPY	<input type="checkbox"/>
INSPECTED	<input type="checkbox"/>
6	
A-1	

LIST OF ILLUSTRATIONS

<u>Figure</u>		<u>Page</u>
1	Illustration of Magnetically Insulated Opening Switch Concept	2
2	Current and Voltage Waveforms in Test Experiments on Magnetic Insulation	2
3	Experimental Apparatus for Study of Magnetic Insulation	3
4	View of the Segmented Anode, Showing Leads to Magnet Coil and Water Cooling Tubes	3
5	View of the Thermionic Cathode Structure Showing Cathode Cylinder at Left	3
6	Idealized Energy Transfer Circuit Using Inductive Energy Storage and Opening Switch	6
7	Optimum Efficiency of Energy Transfer as a Function of Open to Closed Impedance Ratio R	6
8	Efficiency of Energy Transfer as a Function of Output Voltage, at Different Electric Stress Values	6
 Appendix		
1	Details of Diode Configuration	16
2	General View of Diode Configuration	16
3	Circuit Diagram of Experiment	17
4	Typical Diode Current and Voltage Waveforms (1 μ sec Line, 0.15 cm gap)	17
5	Illustration of End Barriers for Axial Electron Containment (a) Diode Configuration with End Barriers, (b) Details of End Barrier Construction	19
6	Diode Perveance for Zero Magnetic Field (0.15 cm gap)	19
7	Diode Current in Magnetically Insulated State (a) Diode Current vs Magnetic Field Strength (0.15 cm gap, 1 μ sec line), (b) Diode Current vs Magnetic Field Strength (0.3 cm gap, 1 μ sec Line)	21

<u>Figure</u>		<u>Page</u>
8	Normalized Diode Current and Magnetic Field Strength for 0.15 cm and 0.3 cm gaps	22
9	Diode Current vs Magnetic Field Strength (0.15 cm gap, 6 μ sec line)	22
10	Diode Current vs Magnetic Field Without End Barriers (0.15 cm gap, 1 μ sec line)	23
11	Geometry for derivations of Equilibrium Flow	23
12	Equilibrium Fields and Electron Density (0.15 cm gap, 895 kG, $V_0 = 35$ kV)	27
13	Cutoff Voltage vs Magnetic Field Strength (0.15 cm gap)	27
14	Probe Configuration for Wave Measurements	30
15	Typical Probe Signals for (a) 1 GHz bw Oscilloscope, (b) Crystal Detector, (c) 3 MHz bw Spectrum Analyzer	30
16	Typical Frequency Spectrums for two Values of A-K Voltage and Magnetic Field Strength	32
17	Wavenumber vs Frequency for the Two Cases Shown in Fig. 16	32
18	Probe Signal Amplitude for Various Experimental Conditions	34
19	Natural Logarithm of Probe Signal Amplitude vs X^*/d (0.3 cm gap)	35
20	Plots of $\ln(I)$ vs x^*	37
21	Configuration of Previous Magnetron Experiments	38
22	Magnetron Leakage Current vs Magnetic Field Strength (replotted from Fig. 3 of Jepsen et. al.)	38
23	Plots of $\ln(I)$ vs x^* for AD9-66E Data of Fig. 22	39
24	$X^* \rightarrow 0$ Intercept Current to the 2/3 Power vs K-K Voltage for Present Experiment and Experiment of Jepsen et. al	39
25	$\ln(I)$ vs x^* for Marconi CW-10 Magnetron Data at 100 V	40
Table 1	Experimental Data	42

1.0 INTRODUCTION

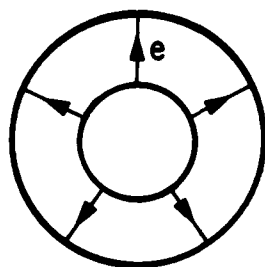
The aim of this research is to investigate the validity of the magnetically insulated opening switch concept proposed by Eninger (Ref. 5, Appendix 1). The device consists of a cylindrical vacuum diode of high aspect ratio, that is, its radius greatly exceeds the anode-cathode gap dimension. In its 'closed' or conducting state electrons are emitted from a thermionic cathode and traverse to the anode obeying (almost exactly) the planar Child-Langmuir relation

$$J_{CL} = \frac{2.33 \times 10^{-6} V^{3/2}}{d^2}$$

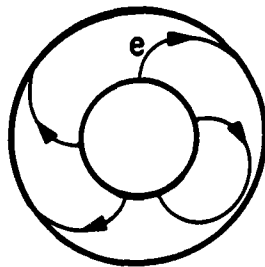
where J_{CL} is the current density (Am^{-2}), V is the anode-cathode voltage and d is the anode-cathode gap in meters.

The switch is changed to its 'open' or insulating state by the sudden injection of an axial magnetic field into the interelectrode gap, which causes the electrons to drift azimuthally without reaching the anode (Fig. 1). In practice there is a small but definite leakage between cathode and anode due to the existence of plasma waves driven by shear in the electron flow. In a detailed series of experiments, described fully in Appendix I, we have shown that the insulated state leaks current at a predictable rate which depends on the voltage V , gap d and magnetic field B . We have also demonstrated stable, long-term insulation ($t > 500$ nsec) at an electric field in the gap averaging 300 kV cm^{-1} .

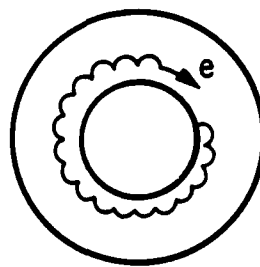
Typical voltage and current waveforms which demonstrate opening switch action are shown in Fig. 2. In that set of traces a current of 350 A initially conducted through a closed impedance of 8Ω is interrupted by an 8 kG magnetic field in $0.5 \mu\text{sec}$ to an insulated voltage of 60 kV and open impedance of 480Ω . The 100 cm^2 test switch apparatus is described in detail in Appendix I. A general view of the experiment is shown in Fig. 3, and additional photographic views of the anode and cathode are shown in Fig. 4 and Fig. 5.



a) $B=0$



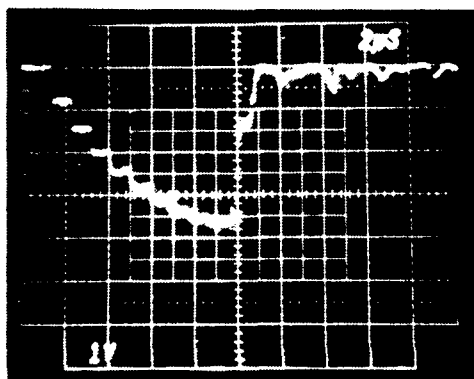
b) $B \approx B_c$



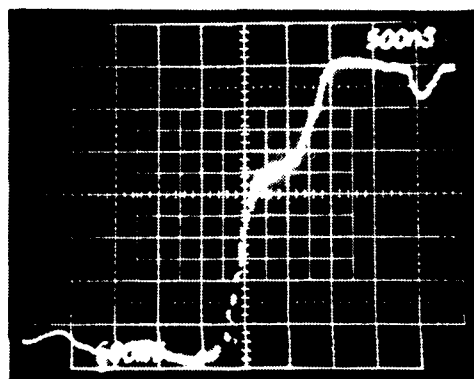
c) $B > B_c$

K6402

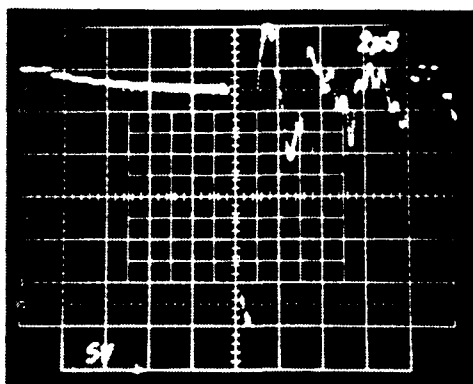
Figure 1 Illustration of Magnetically Insulated Opening Switch Concept



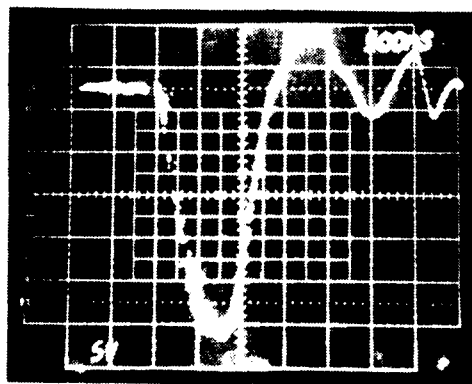
(a) DIODE CURRENT 100 A/div



(b) DIODE CURRENT 50 A/div



(c) DIODE VOLTAGE 10 kV/div



(d) DIODE VOLTAGE 10 kV/div

M2976

Figure 2 Current and Voltage Waveforms in Test Experiments on Magnetic Insulation. Interruption of 350 A to 60 kV in $< 0.5 \mu\text{sec}$

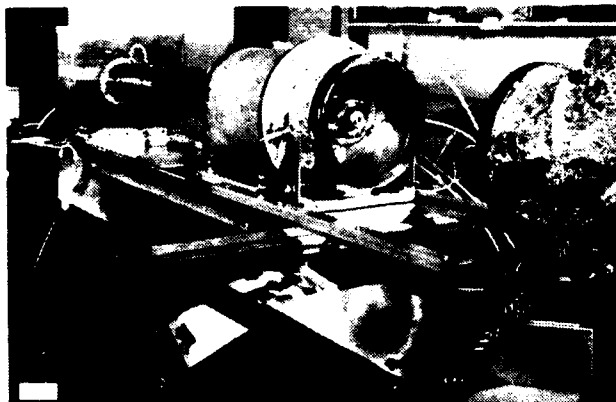


Figure 3 Experimental Apparatus for Study of Magnetic Insulation. Thermionic diode is seen inside vacuum tank. Inductive line is at upper left.

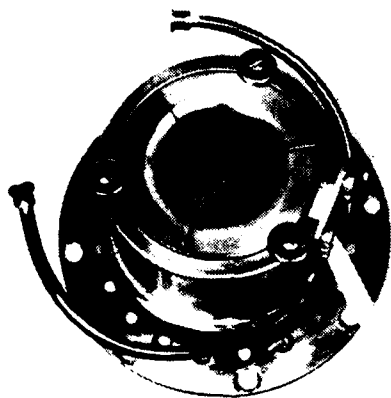


Figure 4 View of the Segmented Anode, Showing Leads to Magnet Coil and Water Cooling Tubes

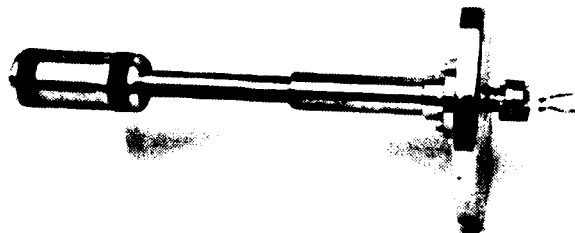


Figure 5 View of the Thermionic Cathode Structure Showing Cathode Cylinder at Left

The leakage data is sufficiently regular and complete as to allow a precise projection of energy transfer efficiency using this switch concept to be made for a general system with intermediate inductive energy storage. This analysis is given in the following section. We note in summary that optimized transfer efficiencies approaching 80 percent are possible at an output voltage of 10 kV. However the transfer efficiency decreases at higher voltages, becoming as low as 20 percent at 1 MV.

2.0 EFFICIENCY SCALING OF MAGNETICALLY INSULATED OPENING SWITCH

The scaling laws that have been determined for leakage in magnetic insulation (Appendix I) have certain consequences for the efficiency of energy transfer of a device based on this principle. As we show in the present section an impedance ratio approaching 10^4 is desirable for really efficient use of an opening switch in inductive energy storage and transfer. We have found experimentally that the impedance ratio of the vacuum diode with magnetic insulation increases as the open voltage is reduced, and at 10 kV open voltage the ratio is of the order of 10^3 , rising to a value which is limited by the electric field which can be stably maintained across the gap.

As a preliminary we discuss the idealized energy transfer circuit of Fig. 6. Initially the capacitor C is charged and switch S is open. With the opening switch 'closed', switch S is closed to transfer energy from C to L. The opening switch is then 'opened' to direct the current stored in L to the load, and the whole cycle is repeated. We define the following quantities:

R = ratio of opening switch 'open' to 'closed' impedances

Z_o = opening switch 'open' impedance

Z_c = opening switch 'closed' impedance

Z_L = load impedance (assumed steady)

ξ = ratio of inductive line 'charge' to 'discharge' time

$R_o = Z_o / Z_L$

$R_c = Z_L / Z_c$

We also assume as a good approximation that the inductive line impedance is matched to the load impedance. With a little calculation we may then show that the efficiency of energy transfer from the capacitor C to the load Z_L is given by

$$\eta = \frac{4R_o^2 (1+R_c)}{(2R_o+1)^2 [(2\xi+1) + R_c]} \quad (1)$$

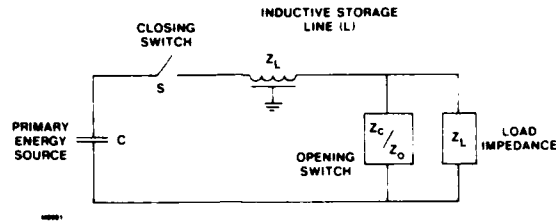


Figure 6 Idealized Energy Transfer Circuit Using Inductive Energy Storage and Opening Switch

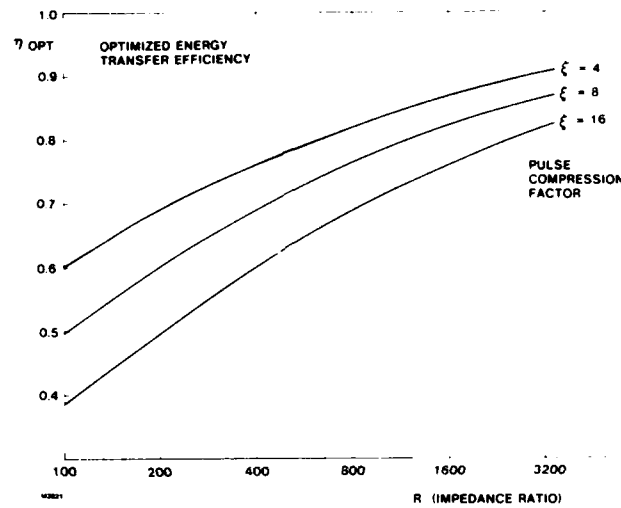


Figure 7 Optimum Efficiency of Energy Transfer as a Function of Open to Closed Impedance Ratio R

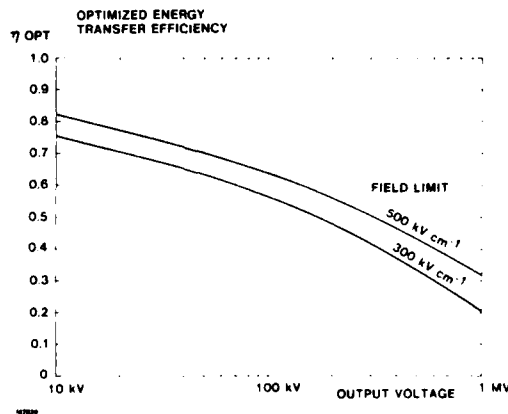


Figure 8 Efficiency of Energy Transfer as a Function of Output Voltage, at Different Electric Stress Values

The losses of energy during the transfer come from three sources:

- (a) Dissipation in the opening switch when it is 'closed'.
- (b) Dissipation in the load when the opening switch is 'closed'.
- (c) Dissipation in the opening switch when it is 'open'.

It is assumed here that the opening switch is rapidly acting, so that dissipation during commutation is negligible (the magnetic switch has been demonstrated to open in $< 1 \mu\text{sec}$), and that it does not matter that there is dissipation in the load prior to the switching of the inductively stored energy.

In general we can optimize η subject to the constraint that $R = R_o R_c$ is a constant. This leads to

$$\eta_{\text{OPT}} = \frac{\frac{2R}{\xi} (1 + \sqrt{2R\xi})}{(2\sqrt{R/2\xi} + 1)^2 [(2\xi + 1) + \sqrt{2R\xi}]} \quad (2)$$

with optimized impedance ratios

$$R_o = \sqrt{\frac{R}{2\xi}} \quad R_c = \sqrt{2R\xi} \quad (3)$$

As a check we note that $R \rightarrow \infty \Rightarrow \eta_{\text{OPT}} \rightarrow 1$, which is the case of an ideal opening switch. In practice the existence of a finite impedance ratio reduces η , as illustrated in Figure 7 for specific values of pulse compression factor in equation (2). As an example, the use of $\xi = 10$ implies $R > 6,400$ for $\eta_{\text{OPT}} > 90\%$, illustrating the need for very high impedance ratios.

With the above discussion as background we now examine the efficiency of an opening switch based on magnetic insulation. For this device the 'closed' diode current I_c is given accurately by the planar Child-Langmuir relation

$$I_c = \frac{\alpha A V_c^{3/2}}{d^2}, \quad \alpha = 2.33 \times 10^{-6} (\text{M.K.S.}) \quad (4)$$

in which V_c is the 'closed' anode-cathode voltage and A and d are the diode area and gap spacing respectively.

The 'open' diode current I_o is given by (Appendix 1)

$$I_o = \frac{\beta A V_o^{3/2}}{d}, \quad \beta = 0.84 \times 10^{-6} \text{ (M.K.S.)} \quad (5)$$

In (5) we have taken the limiting leakage at high magnetic field when the radial extent of the electron cloud (x^*) becomes much less than the gap spacing.

The impedance ratio is then given by

$$R = \frac{\alpha}{\beta d} \left(\frac{V_c}{V_o} \right)^{1/2} \quad (6)$$

If we then express V_c in terms of V_o as

$$V_c = \frac{V_o (1 + 2R_o)}{R_o (1 + R_c)} \quad (7)$$

we obtain

$$R = \frac{\alpha}{\beta d} \left[\frac{1 + 2\sqrt{R/2\xi}}{\sqrt{R/2\xi} (1 + \sqrt{2R\xi})} \right]^{1/2} \quad (8)$$

which determines the available R in terms of the given parameters ξ and d , and the fixed constants α and β . Expression (8) may be approximately solved for R in the limiting case $R \gg \xi \gg 1$, to give

$$R = \left(\frac{2}{\xi} \right)^{1/5} \left(\frac{\alpha}{\beta d} \right)^{4/5} \quad (9)$$

Substituting the known values of α and β we obtain

$$R = 2.6 \xi^{-1/5} d^{-4/5} \quad (10)$$

The impedance ratio R which gives optimum energy transfer therefore depends weakly on the time compression factor ξ , but strongly on the anode-cathode spacing d . As an example, consider $\xi = 10$ and $d = 0.5 \times 10^{-3}$ m, then $R = 716$, and from Figure 7, $\eta_{OPT} = 0.73$.

Finally, the required output voltage V_o together with the allowable electric field set the minimum d that can be used. For example, an electric field of 300 kV cm^{-1} has been demonstrated experimentally (Appendix 1). The factors which limit the electric field have not been explored much in the present work and ought to be addressed in future work to improve this opening switch's efficiency. It is possible that future experiments will yield higher allowable electric fields and consequently higher energy transfer efficiency. Figure 8 shows the efficiency of energy transfer as a function of output voltage, under different assumptions of maximum allowable electric field.

APPENDIX I
EXPERIMENTAL STUDY OF MAGNETIC INSULATION

Paper Accepted for Publication in "The Physics of Fluids"

EXPERIMENTAL STUDY OF MAGNETIC INSULATION
R. Kraft and M.W. McGeoch

AVCO RESEARCH LABORATORY (TEXTRON)
2385 Revere Beach Parkway
Everett, MA 02149

ABSTRACT

An experimental study is made of magnetically insulated electron flow in a cylindrical thermionic diode. Emphasis is laid on measurements of plasma waves and leakage current in the insulated state.

It is found that over a wide range of conditions the leakage current can be represented by

$$I = \frac{0.84 \times 10^{-6} \xi A_c V^{3/2}}{d_{\text{eff}}} \exp \left\{ \frac{4015 x_*}{\xi} \right\} \text{ Amps}$$

where A_c is the cathode area, V the anode-cathode voltage, d_{eff} is an effective interelectrode gap (m), and x_* is the thickness of the Brillouin layer in contact with the cathode (m). ξ is a geometrical factor equal to unity in the present nearly planar geometry, increasing to 3 as the cathode radius becomes much less than the anode radius, as is the case in prior magnetron data also fitted by this formula.

Unstable electrostatic, transverse magnetic (TM) waves are observed at frequencies predominantly below the electron cyclotron frequency with wavelengths equal to the $\pi d/n$ where d = diode diameter, $n = 1, 2, 3, \dots$. The waves are believed to be driven unstable by a resistive wall instability. The correlation between the leakage current and the wave amplitude is discussed.

1.0 INTRODUCTION

Interest in the flow and stability of electrons in crossed electric and magnetic fields has increased in recent years due to applications in magnetically insulated transmission lines,¹ magnetically insulated ion diodes,² rotating hollow electron beams in a guiding magnetic field,³ magnetrons⁴ and magnetically insulated opening switches.⁵

An extensive amount of theoretical work on cross field flow has been performed which builds upon earlier theoretical analyses.⁶⁻⁸ Unfortunately, there have been few experimental studies to enable a comparison with theory. This paper presents experimental observations of electron flow and stability in crossed electric and magnetic fields and compares these results with recent theoretical models.

Most theoretical work is based upon a flow model in which electrons undergo laminar drifts at the local $\underline{E} \times \underline{B}$ velocity. The diode studied in this paper is modeled as a $q = (\omega_{pe}/\Omega_{ce})^2 = 1$ device. The electron flow is laminar and sheared because the electron space charge modifies the local electric field. A detailed discussion of the electron flow will be presented in Section 4.

Recent theoretical studies of linear waves and instabilities in a sheared ($q = 1$) laminar flow⁹⁻¹³ have revealed; (a) electrostatic (TM) waves propagating perpendicular to the magnetic field exhibit the largest growth rate, (b) a long wavelength instability (the diocotron instability) is stabilized when the electron layer is bounded by a conducting cathode which prevents interaction between surface waves at opposite electron layer surfaces, (c) a short wavelength instability (magnetron instability) occurs when electron layers obeying $\omega = kV_z$ and $\omega = kV_z + \Omega_{ce}$ (V_z is electron drift velocity) both exist and (d) if the anode has finite resistivity an instability (resistive wall instability) occurs at frequencies below the electron cyclotron frequency.

In the present experiment, unstable TM waves (Section 5) were observed predominantly below the electron cyclotron frequency indicating a resistive wall instability. In Section 6, experimental measurements of the leakage current are discussed in relation to the unstable wave measurements. Finally, the results of these sections are summarized in Section 7.

2.0 EXPERIMENTAL APPARATUS

Electron motion is studied in a coaxial cylindrical vacuum diode which has a thermionic cathode as the inner cylinder and a copper anode as the outer cylinder. In these experiments the cathode dimensions remain fixed at 5.1 cm diameter and 6.3 cm length. The cathode material is sintered tungsten impregnated with barium oxide (Spectramat). Cathode emission of up to 10 A/cm^2 is obtained in a vacuum of $\sim 1 \times 10^{-6}$ torr at 1200°C .

Two anodes types were utilized, one with three axial slots and one with a single axial slot. The slots allowed the magnetic field to penetrate into the anode-cathode gap. The arrangement is shown in Figure 1, where the winding which generates the pulsed magnetic field can be seen outside the anode. The anode-cathode gap is varied by using anode structures with different internal diameters. In the present work, anode-cathode spacings of 0.15 cm and 0.3 cm have been used. The anode is mounted at its ends to a copper outer case which encloses the anode winding. This contact provides cooling of the anode segments and the electrical ground connection. The cathode is suspended on a graded ceramic bushing rated at 200 kVdc as shown in Figure 2.

The electrical test circuit is shown in Figure 3. It consists of a capacitor (C_1) and inductive storage line (L_1) which are switched by grounded-grid thyatron through the vacuum diode. Two different lines were used in the measurements: the 1 μsec , 300 Ω line shown in Figure 3 and a 6 μsec , 250 Ω line of total inductance 805 μH . The inductive lines were bifilar wound to carry the cathode heater current of 17 A (60 Hz, 55 V). The establishment of the peak current through the diode took 10 μsec or 25 μsec , respectively, after which time the magnetic field pulser was fired.

In the case of the 1 μsec line the magnetic pulser capacity ($C_2 = 0.6 \mu\text{F}$) created a current up to 13 kA through the anode winding with a period of 3 μsec and generated a magnetic field up to 8 kG. With the 6 μsec line, the number of turns on the anode winding was approximately doubled and the pulser capacity increased ($C_2 = 3 \mu\text{F}$) giving a magnetic field up to 13 kG with a period of 12 μsec .

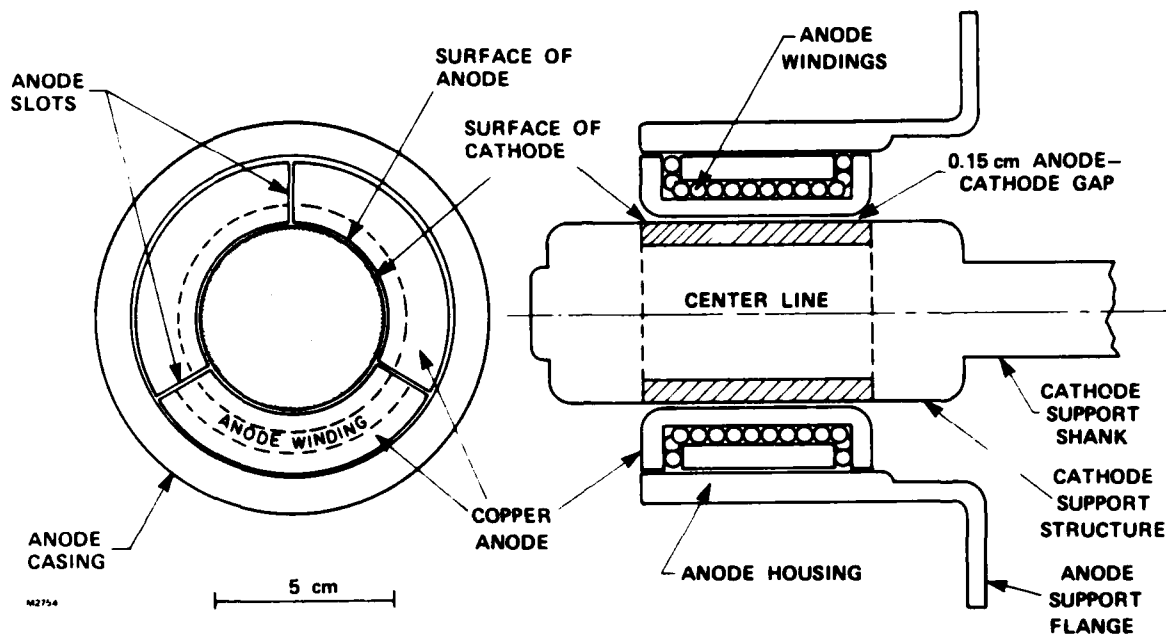


Figure 1 Details of Diode Configuration

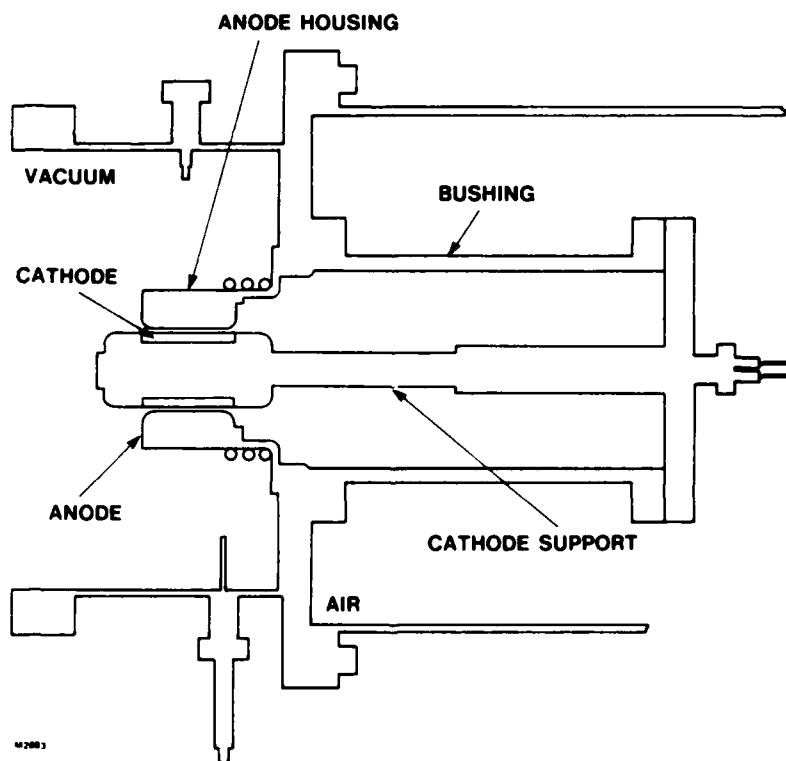


Figure 2 General View of Diode Configuration

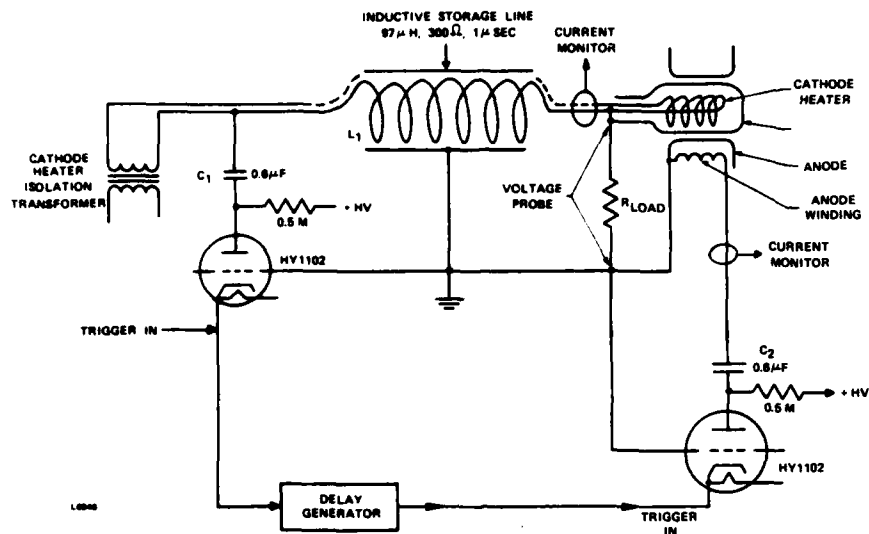


Figure 3 Circuit Diagram of Experiment

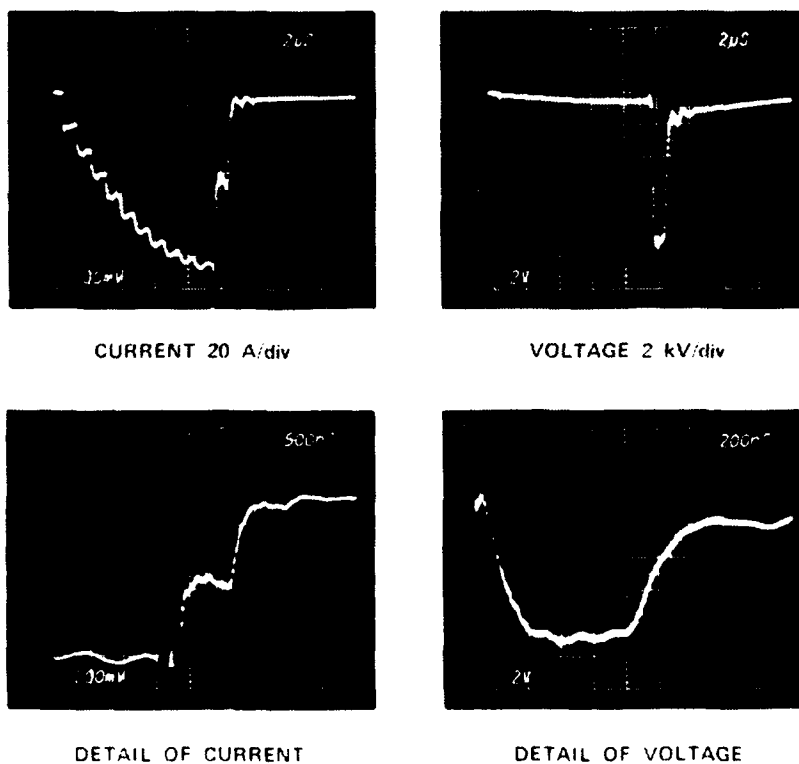


Figure 4 Typical Diode Current and Voltage Waveforms (1 μsec line, 0.15 cm gap)

When the magnetic field in the diode exceeded the critical value for insulation, the diode impedance rapidly rose causing the inductive line to discharge as a transmission line. The diode impedance maintained a constant value for ~ 600 nsec with the $1 \mu\text{sec}$ line and $3 \mu\text{sec}$ with the $6 \mu\text{sec}$ line. During this time the inductive line was driving a constant load ($R_L = 10 \text{ k}\Omega \parallel R_{\text{diode}}$) and therefore generated a constant voltage pulse. Typical waveforms of diode voltage and current are shown in Figure 4 for the $1 \mu\text{sec}$ line.

It was found that suitably designed end barriers could greatly reduce electron leakage from the cathode. These barriers, or "end caps," have the same function as cathode "hats" in magnetron design, but owing to the rapidly rising magnetic field the details of their construction have to be different. The barriers function by allowing magnetic field penetration during the field risetime, but are made of conducting material so that electrons traveling toward the barrier are reflected at the cathode potential. The barriers used in the experiment (Figure 5) were constructed of 1 mil molybdenum and slotted to allow rapid penetration of the magnetic field on the time scale of the magnetic field pulse.

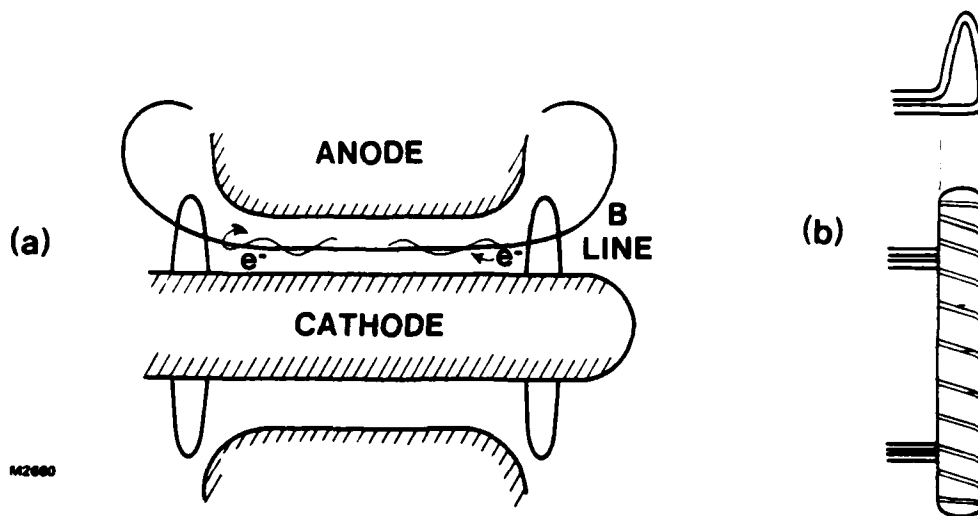


Figure 5 Illustration of End Barriers for Axial Electron Containment
 (a) Diode Configuration With End Barriers,
 (b) Details of End Barrier Construction

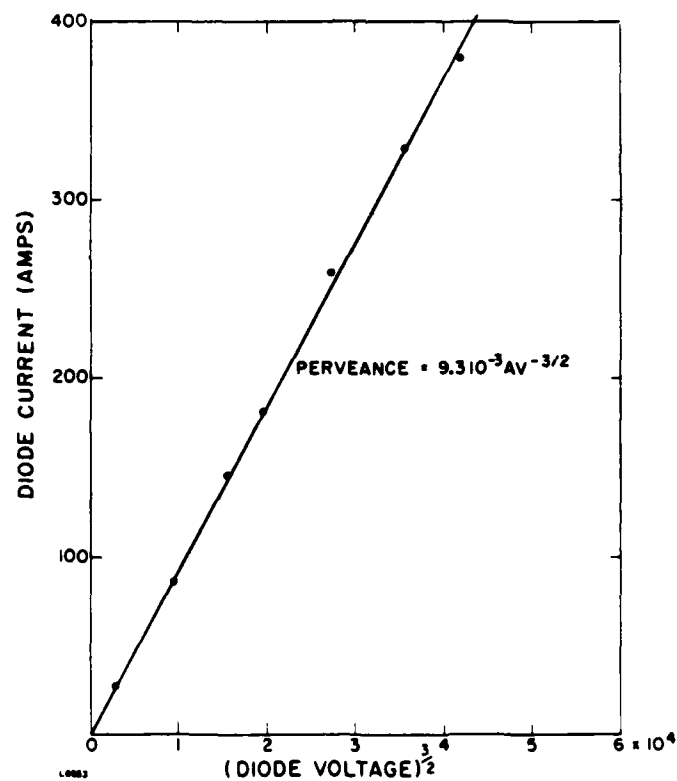


Figure 6 Diode Perveance for Zero Magnetic Field (0.15 cm gap)

3.0 DIODE CHARACTERIZATION

For each of the two anode-cathode spacings the crossed field leakage current was measured as function of magnetic field and anode-cathode voltage. The details of these measurements are given in the present section.

As a test of cathode emission and recording calibration the diode characteristics were measured with zero magnetic field (Figure 6). The diode permeance was within 2 percent of that calculated for the 0.15 cm gap, with an effective diode area of 90 cm^2 . Cathode emission of up to 5.8 A/cm^2 was recorded, with no sign of saturation.

For a given magnetic field strength, the voltage generated across the diode could be varied by changing the current through the diode prior to pulsing the magnetic field. This was accomplished by changing the charge voltage on C_1 in Figure 3.

The leakage current (measured at $B=0$) as a function of the peak magnetic field strength for various A-K voltages is shown in Figure 7. These curves can be replotted as leakage current divided by the Child-Langmuir current vs magnetic field divided by critical magnetic field (Figure 8). The leakage current rapidly decreases from the Child-Langmuir value, I_{C1} , to ~ 0.0035 (0.001) I_{C1} for the 0.03 (0.15) cm gap as the magnetic field is increased above the critical value.

With the 6 μsec line (Figure 9) the leakage was almost identical to that with the 1 μsec line. At high magnetic fields the leakage (measured at $B=0$) with the 6 μsec line exceeded the 1 μsec line leakage (measured at $B=0$) by a factor of ~ 1.2 , apparently due to a partial plasma closure of the leakage path to the anode.

Diode leakage without end barriers was substantially in excess of that with barriers by almost an order of magnitude (Figure 10). In this case the leakage is attributed to an unimpeded flow down the magnetic field lines to the grounded anode casing. To minimize electron leakage out of the ends of the diode, the end barriers were designed to intercept as many of the magnetic field lines from the A-K gap as possible (tall barriers, close to anode). A cylindrical foil of radius 4 cm was mounted close to the end of the anode to

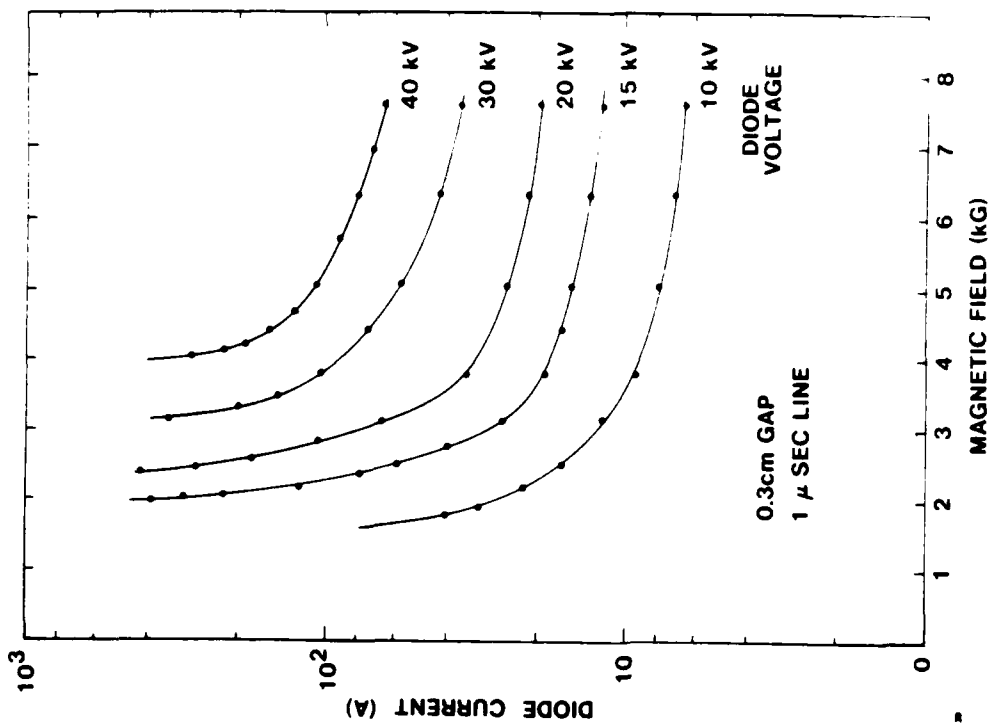
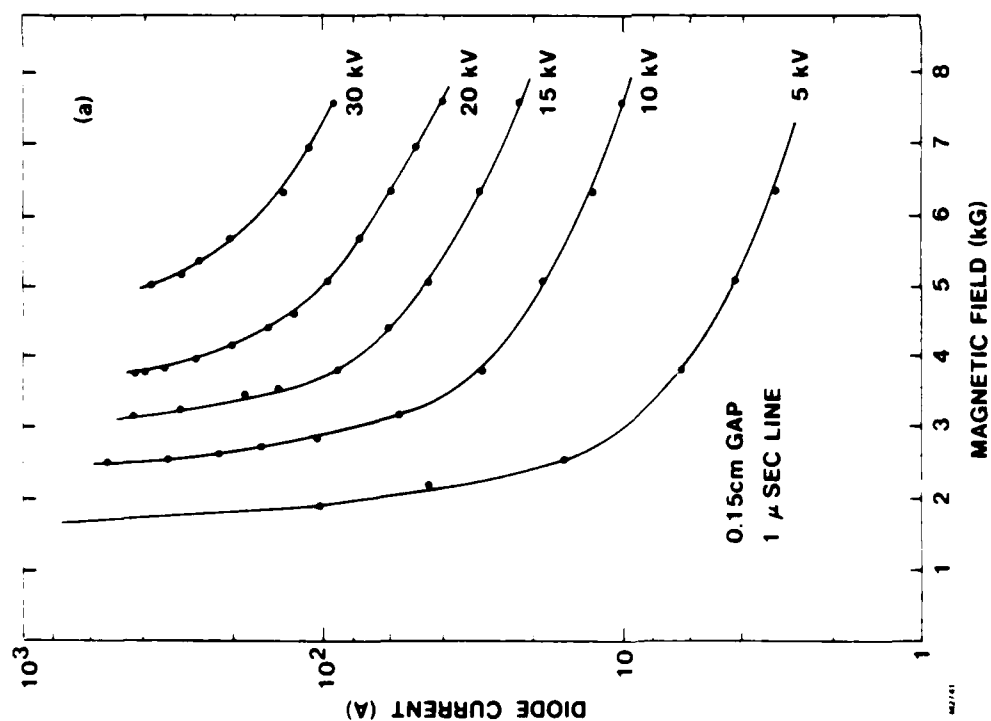


Figure 7 Diode Current in Magnetically Insulated State
 (a) Diode Current vs Magnetic Field Strength (0.15 cm gap, 1 μ sec line), (b) Diode Current vs Magnetic Field Strength (0.3 cm gap, 1 μ sec line)

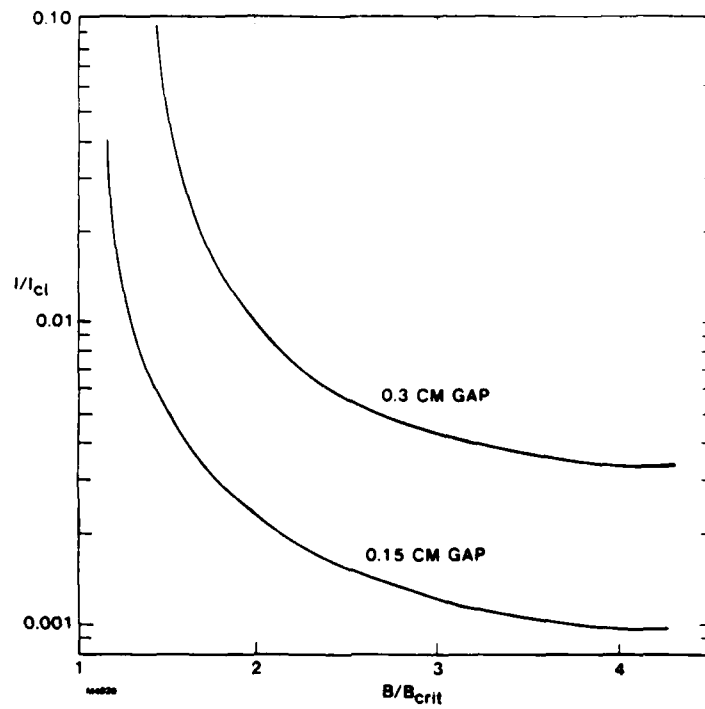


Figure 8 Normalized Diode Current and Magnetic Field Strength for 0.15 cm and 0.3 cm gaps

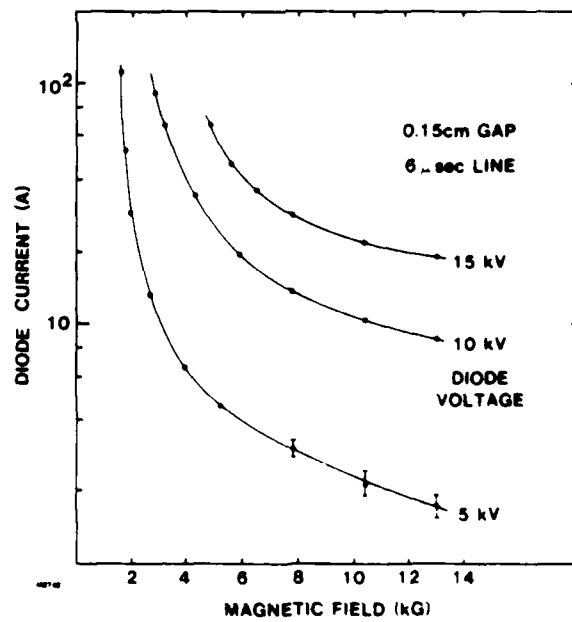


Figure 9 Diode Current vs Magnetic Field Strength (0.15 cm gap, 6 μsec line)

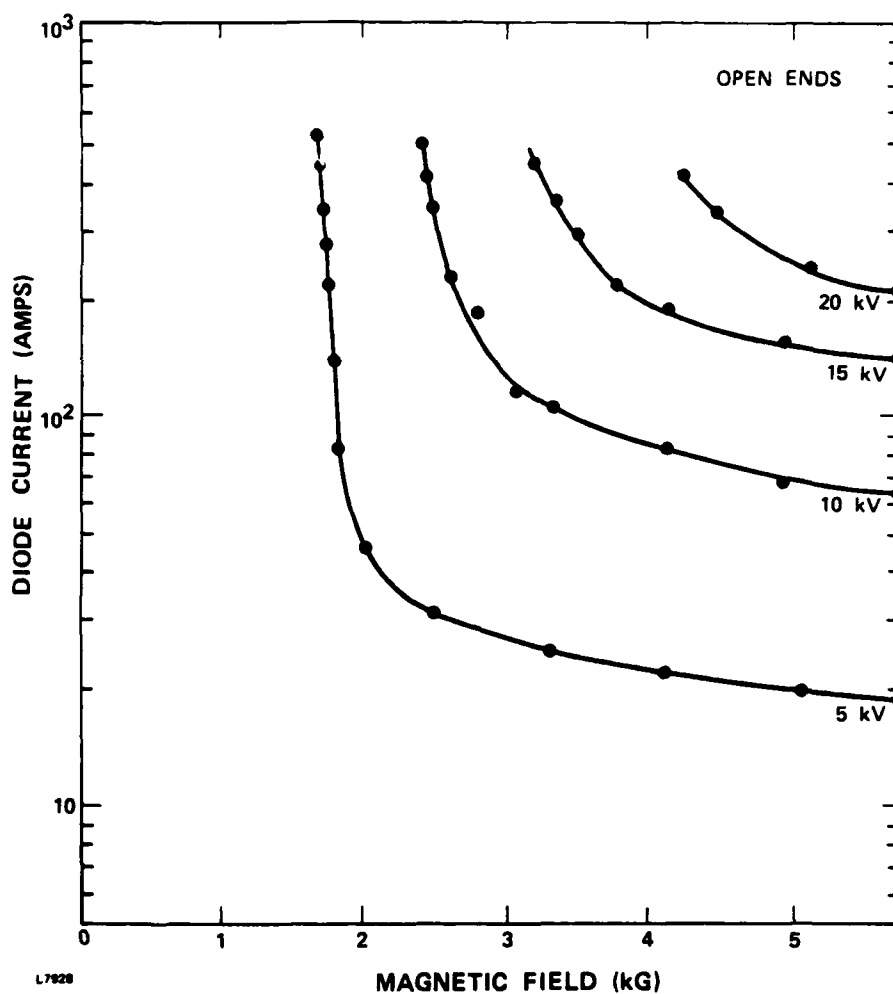


Figure 10 Diode Current vs Magnetic Field Without End Barriers (0.15 cm gap, 1 μ sec line)

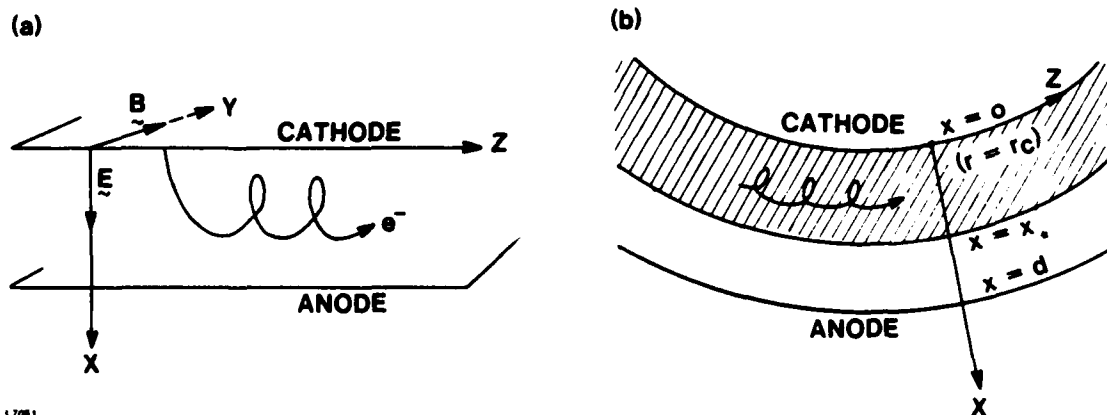


Figure 11 Geometry for derivations of Equilibrium Flow. (a) Planar geometry (b) application to cylindrical geometry, showing electron cloud between $r = r_c$ and $r_* = r_c + x_*$

collect the end leakage current. Using this probe it was verified that the end barriers on the 0.3 cm gap were between 65 percent and 90 percent effective in reducing end leakage, becoming most effective at high magnetic fields.

The highest voltage that could be stably supported across the 0.15 cm gap was 45 kV. Attempts to exceed this voltage led to premature arcing and short circuit of the gap before the peak magnetic field had been reached. On the other hand, the highest stable voltage observed across the 0.3 cm gap was 70 kV. The average electric fields sustained across the two gaps were 300 kV cm^{-1} and 233 kV cm^{-1} respectively. In order to reach such values several thousand pulses were fired in a process of conditioning at gradually increasing electric fields. Typically the repetition frequency was 0.8 Hz, limited by the power supply capacity. After each normal pulse a small increase in chamber pressure from $\sim 8 \times 10^{-7}$ to 1×10^{-6} torr was observed, indicating a gas release of $\sim 5 \times 10^{14}$ molecules per 1 μsec pulse. Following an arc up to ten times more gas could be released.

As a test of the effect of background gas on the leakage current, argon was added to the chamber in a pressure up to $\sim 2 \times 10^{-3}$ torr without any change whatsoever in diode leakage, showing that it is truly an electron phenomenon and not due to plasma closure. In corroboration of this the diode characteristics were found to be extremely stable with time and reproducible within 5 percent on successive days of the experiment.

4.0 LAMINAR FLOW MODEL

The electron flow in the diode was analyzed with the laminar flow model of Lovelace and Ott¹⁴⁻¹⁵ which is appropriate because the voltage risetime on the diode is much longer than a cyclotron period. Considering the planar geometry shown in Figure 11, Lovelace and Ott derived the following expressions describing the equilibrium electron flow from conservation of canonical momentum (MKS)

$$E_x = -k \left(\frac{mc^2}{e} \right) \sinh(kx) \quad (1)$$

$$B_y = k \left(\frac{mc}{e} \right) \cosh(kx) \quad (2)$$

$$V_z = c \tanh(kx) \quad (3)$$

$$n = \frac{mc^2 \epsilon_0}{e^2} k^2 \cosh(kx) \quad (4)$$

$$\Omega_{ce} = \omega_{pe} = kc \quad (q = 1) \quad (5)$$

where m is the electron mass, e the electron charge, V_z is the drift velocity and n is the electron density. These expressions are valid for $0 \leq x \leq x_*$ where x_* is the location of the outer edge of the electron layer. Both k and x_* are functions of the applied voltage and magnetic field and are found by solving

$$\bar{A}_0 = \sinh(kx_*) + k(d-x_*) \cosh(kx_*) \quad (6)$$

$$\bar{V}_0 = \cosh(kx_*) + k(d-x_*) \sinh(kx_*) \quad (7)$$

where $A_0 = eB_y^0 d/mc$ and $V_0 = 1 + eV_0/mc^2$ with B_y^0 and V_0 the applied magnetic field and A-K voltage. Values of magnetic field, electric field and number density are shown in Figure 12 for a specific set of experimental parameters.

Equation 7 can be rewritten as

$$k(d-x_*) = (1 + \bar{A}_0^2 - \bar{V}_0^2)^{1/2} \quad (8)$$

giving the cutoff criterion ($x_* < d$)

$$\left(\frac{eB_y^0 d}{mc}\right)^2 > 2\left(\frac{eV_0}{mc^2}\right) + \left(\frac{eV_0}{mc^2}\right)^2. \quad (9)$$

In the present experiments $eV_0 < 70$ keV, so the second term in the RHS of Eq. (9) is relatively small and the cutoff voltage is proportional to the square of the magnetic field. The cutoff voltage as a function of the applied magnetic field for the 0.15 cm gap is shown in Figure 13.

In cylindrical geometry the insulation criterion is given by Eq. (9) with d replaced by the effective gap¹³ where r_c and r_a are the cathode and anode radii respectively ($r_c < r_a$).

$$d_{\text{eff}} = (r_a^2 - r_c^2)/2r_a \quad (10)$$

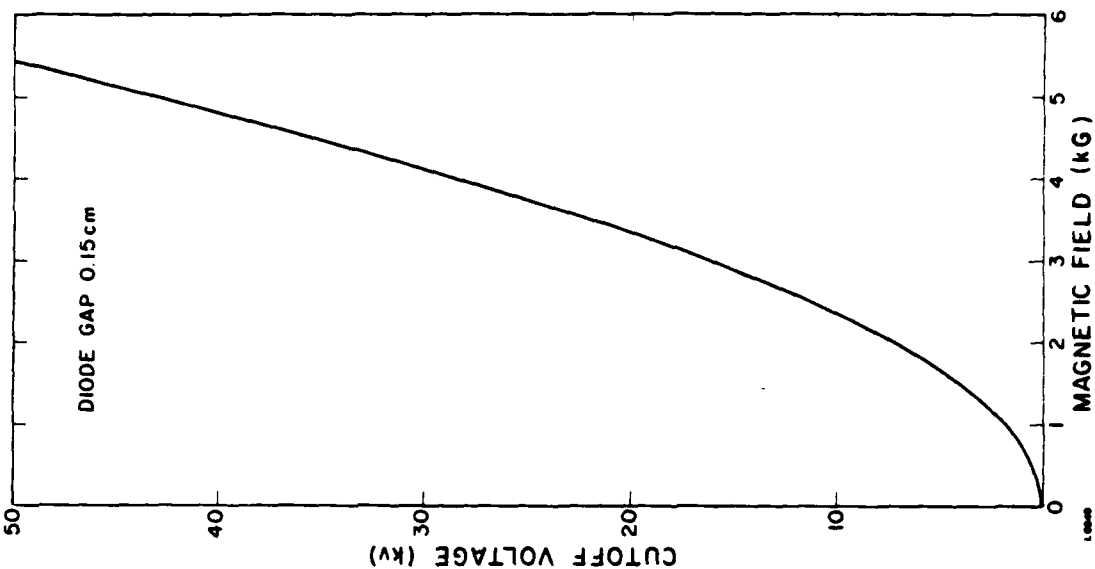


Figure 13 Cutoff Voltage vs Magnetic Field Strength (0.15 cm gap)

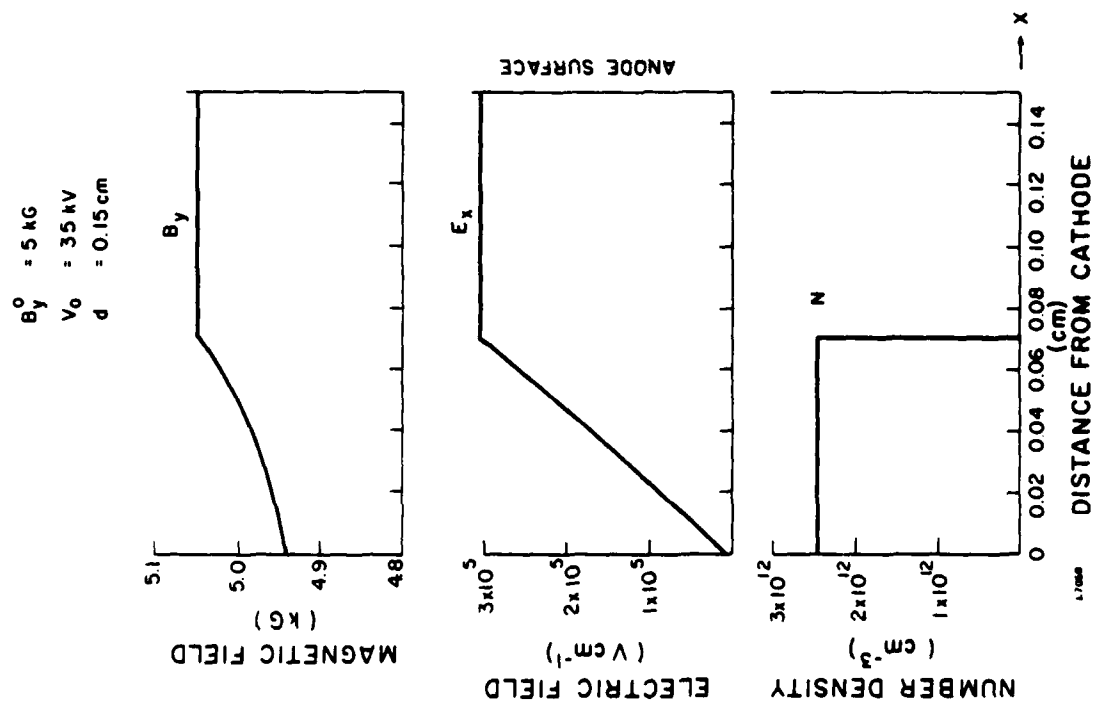


Figure 12 Equilibrium Fields and Electron Density (0.15 cm gap, 895 kg, $V_0 = 35 \text{ kv}$)

The above model for electron flow predicts zero electron current from the cathode to the anode when the magnetic field satisfies Eq. (9). The observed leakage in this experiment is attributed to unstable waves in the electron layer. The experimental investigation of these waves is described in the following section.

5.0 WAVE MEASUREMENTS

Two probes (Figure 14) were located in the anode and the third probe was inserted through one of the end caps. Each anode probe consisted of a 3 mm diameter copper disc recessed ~ 1 mm into the anode and electrically insulated with alumina. The disc was connected to 50 Ω semi-rigid coaxial cable. The probe through the end cap consisted of a section of 50 Ω coax with the center conductor ~ 6 mm longer than the outer conductor. The end of the outer conductor was positioned at the inside edge of the end cap and the inner conductor extended into the A-K gap perpendicular to the electron flow. The outer conductor was electrically insulated with an alumina tube and the inner conductor with a quartz tube. All the probe data was taken at a 0.3 cm anode-cathode spacing and with the 6 μ sec line.

Three methods were employed to observe the signals picked up by the probes; (a) a 1 GHz bw oscilloscope, (b) crystal detectors in combination with various high and low pass filters and (c) a 0-1.8 GHz spectrum analyzer which as operated as a fixed frequency receiver (3 MHz bw).

A typical oscilloscope trace of the envelope of the anode probe signal is shown in Figure 15(a). The signal amplitude is greatest at the beginning and end of the pulse when the magnetic field is close to the critical value ($x_*/d \approx 1$). In the middle of the pulse when the voltage, magnetic field and diode impedance are relatively constant, the signal maintains a uniform lower value.

Using various combinations of high and low pass filters and a calibrated crystal detector (Figure 15(b)) it was found that > 90 percent of the detected power (measured at $B=0$) occurred at frequencies below the electron cyclotron frequency.

To measure the frequency spectrum, the spectrum analyzer was tuned to a specific frequency and ~ 20 pulses were digitally recorded and averaged (signals ranged from 0 to -50 dbm depending on diode operating conditions). The averaged signals (Figure 15(c)) had the same temporal characteristics as the signals observed on the oscilloscope. By tuning the analyzer to various frequencies, the spectrum from 0-1.8 GHz was recorded.

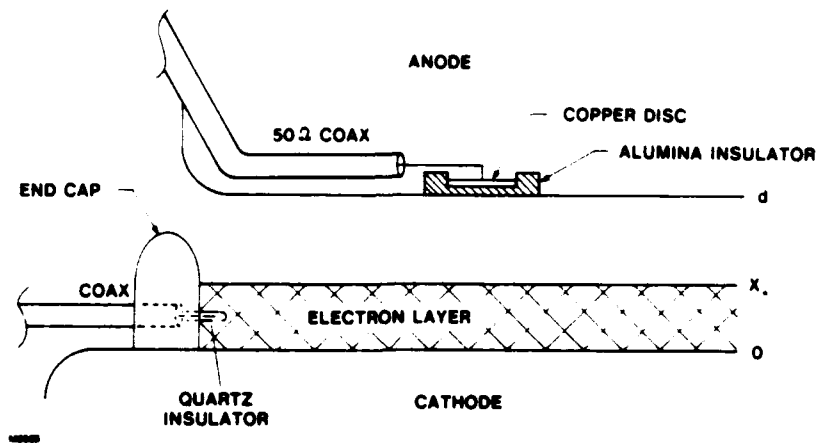


Figure 14 Probe Configuration for Wave Measurements

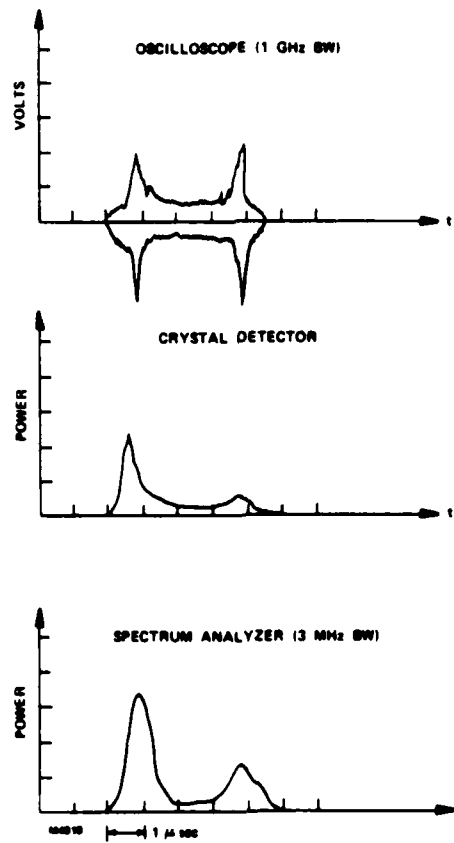


Figure 15 typical Probe Signals for (a) 1 GHz bw Oscilloscope, (b) Crystal Detector, (c) 3 MHz bw Spectrum Analyzer

Figure 16 shows the frequency spectrum for two values of A-K voltage and magnetic field strength. The spectrum has distinct regularly spaced peaks (modes) which correspond to integer number of wavelengths around the circumference. They have been labeled $n = 1, 2, 3, \dots$ corresponding to $\lambda_n = \text{circumference}/n$.

The frequencies observed are well below the cutoff frequency for any waveguide modes associated with the diode structure and are the same for both the single and triple slot anodes. Therefore, we do not believe that the spectrum is influenced by coupling between the electron layer and the slots.

In Figure 17, $1/\lambda_n$ is plotted as a function of the frequency of the n^{th} mode for the two cases of Figure 16. The points fall on straight lines passing through the origin yielding dispersion relations of the form; $f = V_\phi/\lambda$ where V_ϕ is the phase velocity. The phase velocity was approximately equal to the electron velocity at x_* .

It is concluded that the unstable waves are; (a) electrostatic ($V_\phi \sim V_z(x_*) \ll C$), (b) transverse magnetic ($\lambda_n = \text{circumference}/n$) (c) long wavelength ($\lambda \gg x_*$) and (d) low frequency ($\omega < \Omega_{ce}$). To account for these waves, various instability mechanisms were examined. The diocotron instability was ruled out due to fact that the electron layer is bounded by a conductive cathode. The magnetron instability was also ruled out due to the fact that the waves were unstable below the electron cyclotron frequency. The resistive wall instability,¹¹ however, could account for the experimental observations.

The resistive wall instability is caused by a phase lag in the image charges flowing in the resistive anode. This phase lag results in an electric field component E_z^1 , which introduces an $E_z^1 \times B_y^0$ drift. Those electrons which drift toward the anode (leakage current) increase the magnitude of E_z^1 which further increases the drift velocity, the result is instability.

A theoretical analysis by Chernin¹¹ based on the flow model described in Section IV predicts that a resistive anode will cause a long wavelength, low frequency instability ($\omega \lesssim \Omega_{ce}$). The growth rate increases as the edge of the electron layer approaches the anode ($x_*/d \rightarrow 1$) and the instability condition is that a synchronous stream ($V_z(x) = V_\phi$) exists in the unperturbed electron layer.

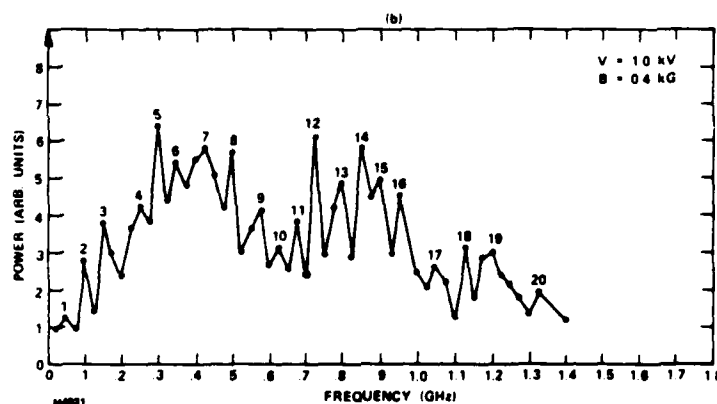
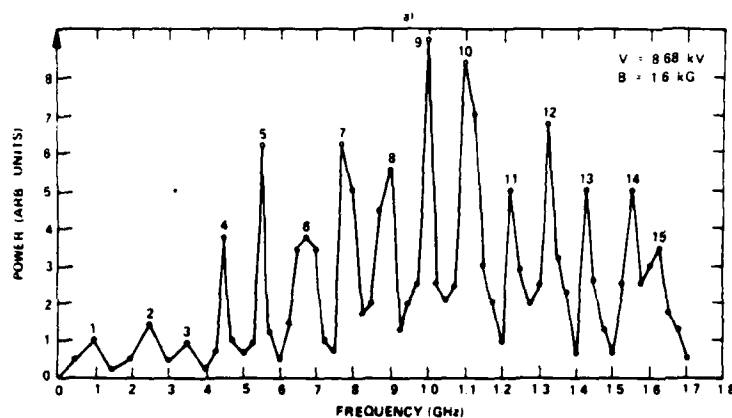


Figure 16 typical Frequency Spectrums for two Values of A-K Voltage and Magnetic Field Strength

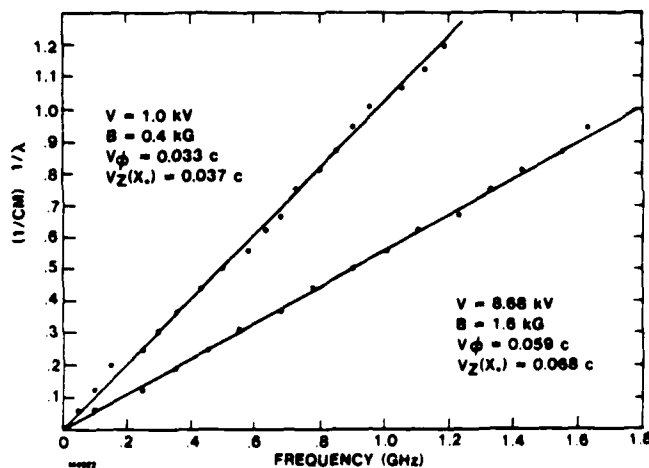


Figure 17 Wavenumber vs Frequency for the Two Cases Shown in Fig. 16

To examine the stability as a function of the electron layer thickness, the amplitude (integrated over frequency) of the probe signal was measured (at $B=0$) as a function of A-K voltage and magnetic field strength (Figure 18). The signal amplitude increased as the voltage was increased (holding magnetic field constant) or as the magnetic field was decreased (holding voltage constant). In other words, the thicker the electron layer, the greater the wave amplitude. This is seen in Figure 19, where the logarithm of the probe signal amplitude is plotted as a function of electron layer thickness as computed from (6) and (7).

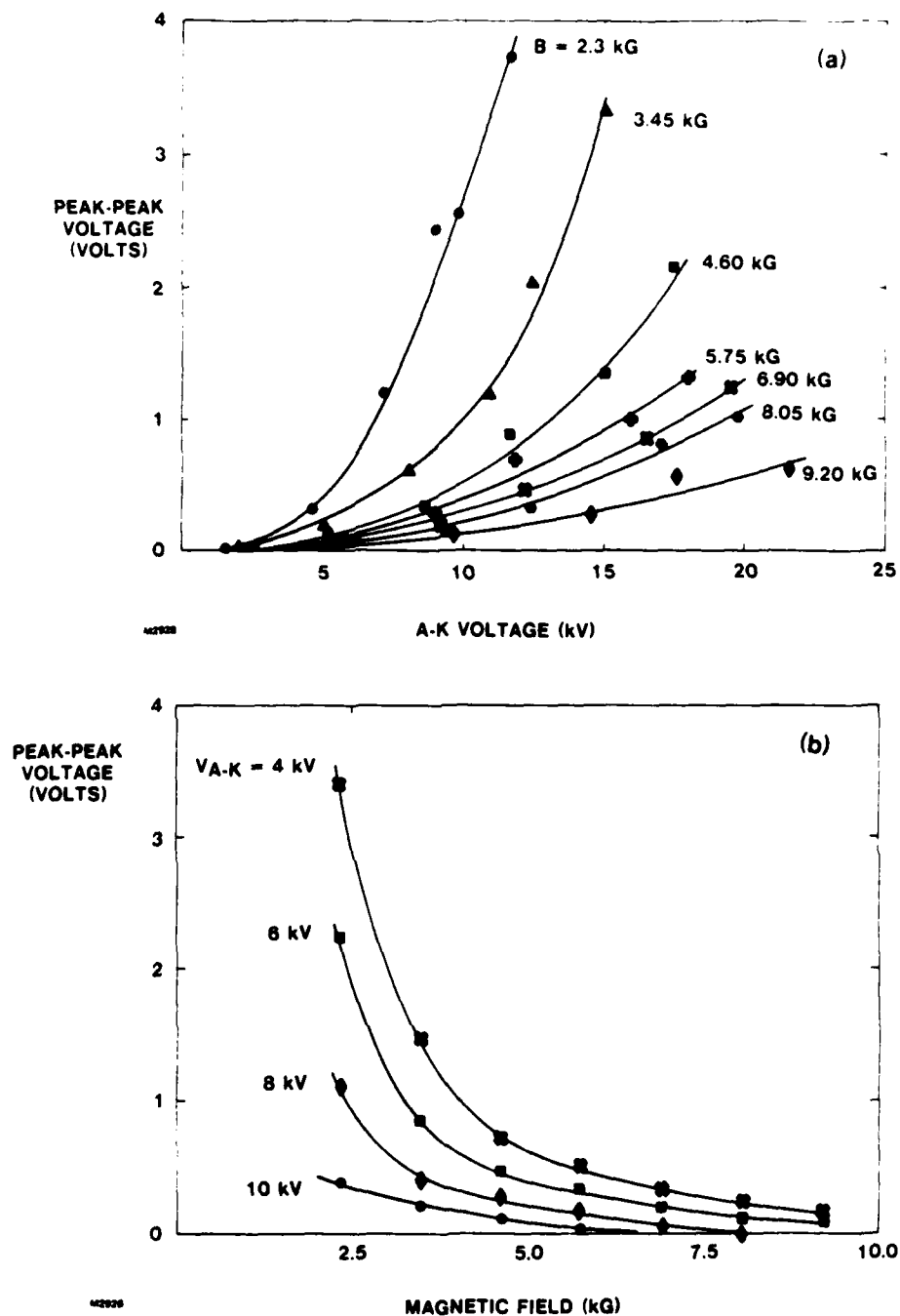


Figure 18 Probe Signal Amplitude for Various Experimental Conditions.
 (a) Probe signal amplitude vs A-K voltage for various magnetic field strengths, (b) probe signal amplitude vs magnetic field strength for various A-K voltages.

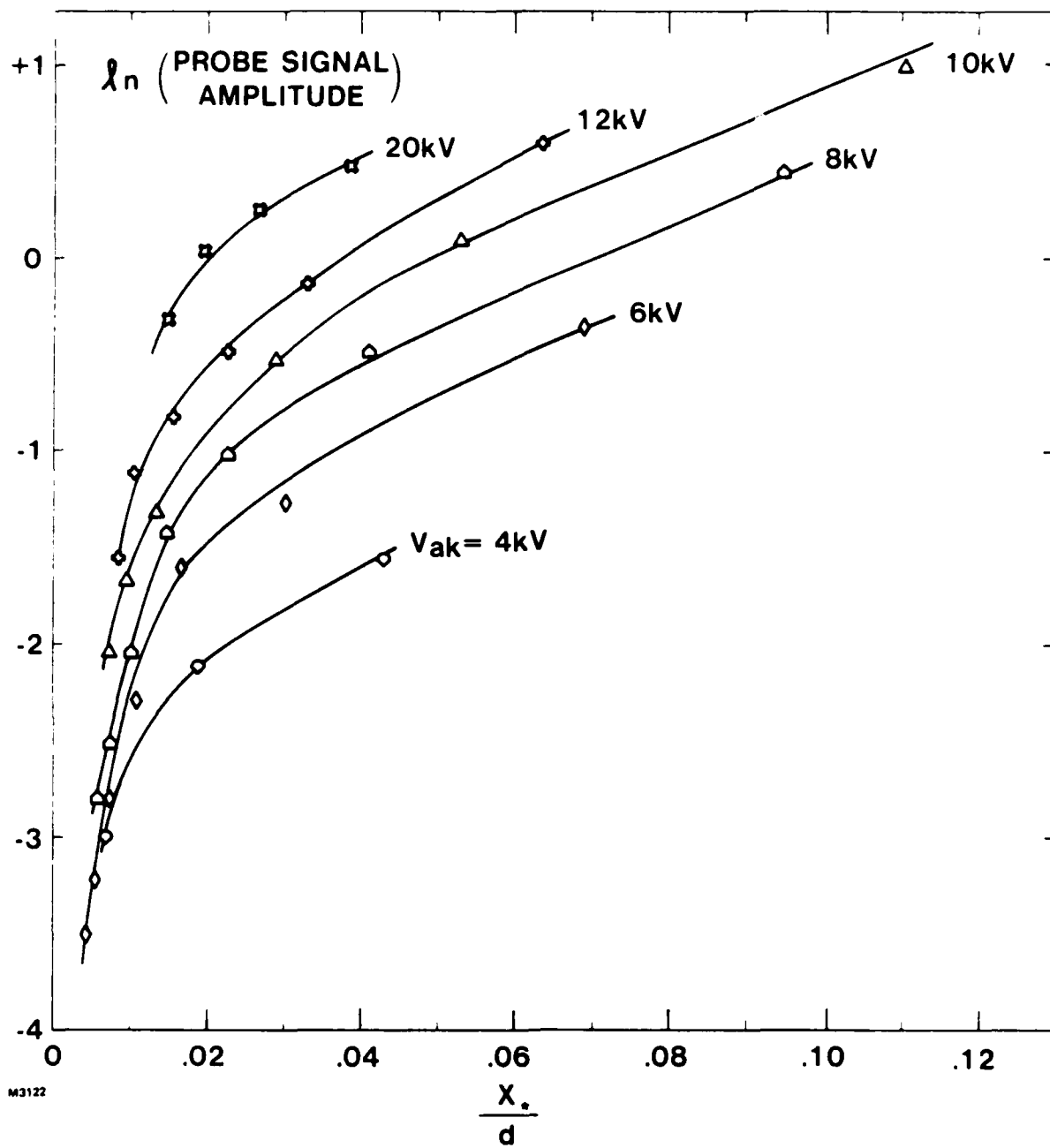


Figure 19 Natural Logarithm of Probe Signal Amplitude vs x_*/d (0.3 cm gap)

6.0 CORRELATION BETWEEN WAVE AMPLITUDE AND LEAKAGE CURRENT

If the leakage current ($E_z^1 \times B_y^0$ drift) in the diode is due to unstable (TM) waves, one would expect a correlation between wave amplitude and current. To make this comparison we examined the two quantities as a function of the thickness of the electron layer x_* .

In Figure 20 the natural log of the leakage current (Figure 7) is plotted as a function of x_* for the two gap spacings. There is a linear dependence for $x_* > 0.05$ cm, more accurately linear at lower voltages.

The lowest voltage regions were used to determine the first two lines in each figure, and the remaining lines were constructed parallel to these, to lie through the data for $x_* > 0.05$ cm. Deviations from a linear dependence of $\ln(I)$ on x_* are mostly on the high side for $x_* < 0.05$ cm, but include a notable departure on the low side at 5 kV on the 0.15 cm gap.

At this point we note that a similar dependence of $\ln(I)$ on x_* also holds for data on a smooth-anode magnetron operated conventionally in a dc magnetic field with ~ 1 μ sec voltage pulses applied between cathode and anode.¹⁶ This magnetron is illustrated in Figure 21(a). Data from Figure 3 of Ref. 16 can be replotted as leakage current at constant voltage vs magnetic field strength (Figure 22). The same data is presented again in Figure 23 where $\ln(I)$ is seen to be linearly dependent on x_* . As in the present experiment, the Jepsen magnetron was believed to have reached steady conditions in times much less than 1 μ sec. Comparing Figure 23 with Figure 20, very close qualitative resemblances are apparent. As discussed below, there also are quantitative similarities.

The voltage dependence of the leakage current is invariant with x_* in all the data. In order to parametrise this dependence we have plotted the 2/3 power of the current intercepts at zero x_* versus voltage in Figure 24. In each case the leakage current intercept depends on voltage to the 3/2 power, with the more accurate dependence shown by the Jepsen magnetron data.

Finally, the data from a very careful series of experiments on magnetron cutoff behavior performed by Harvey¹⁶ also shows a $\ln(I)$ vs x_* linear dependence (Figure 25). This was obtained at 100 V from a continuously oper-

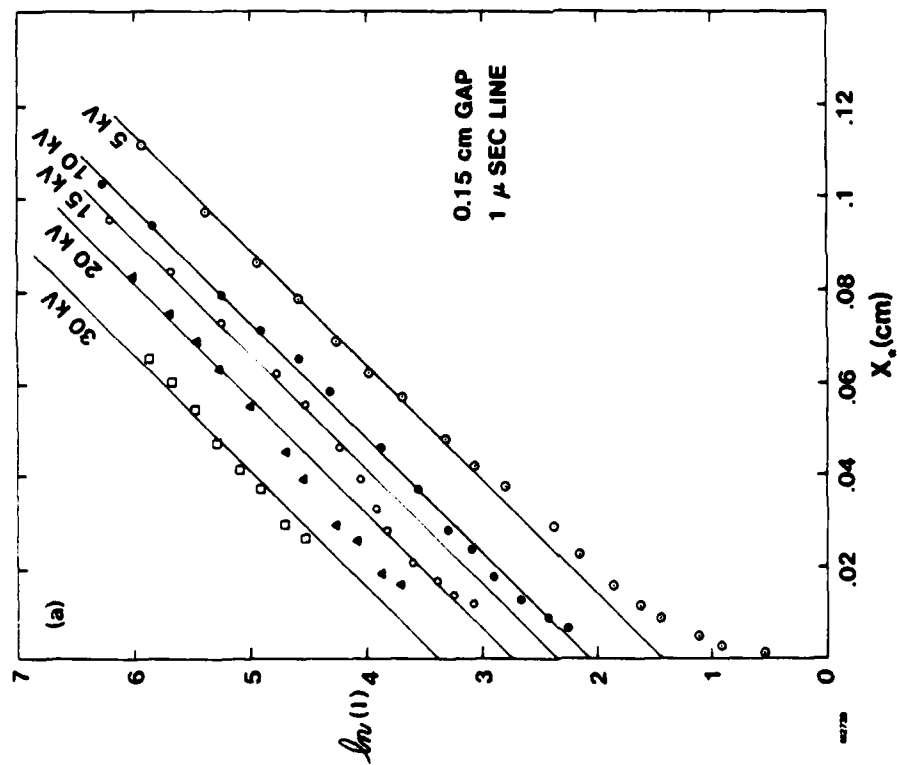
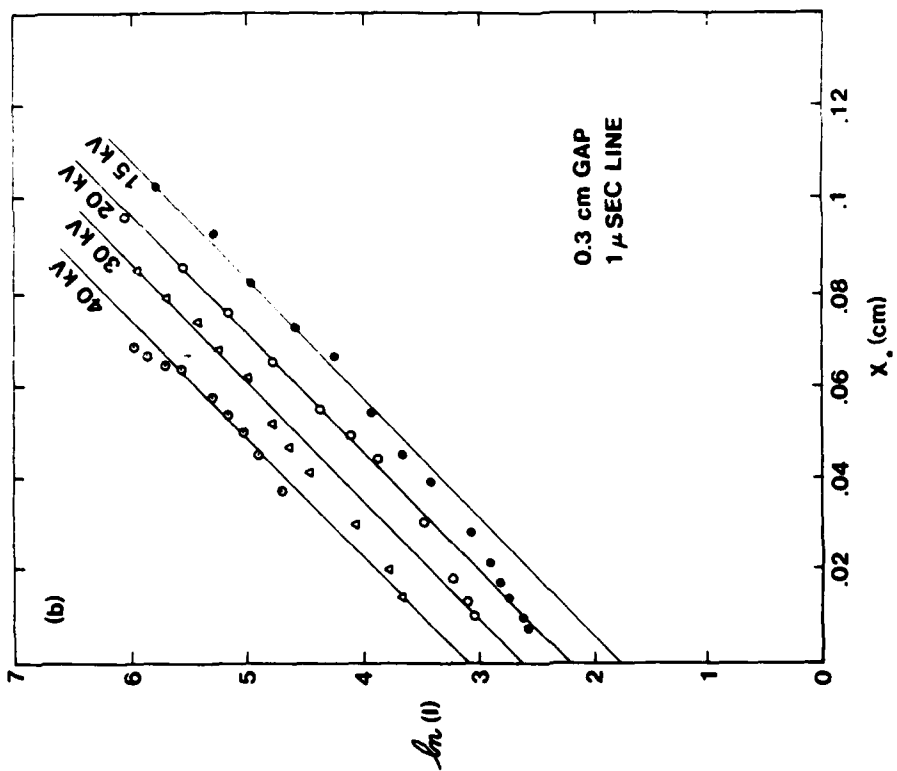
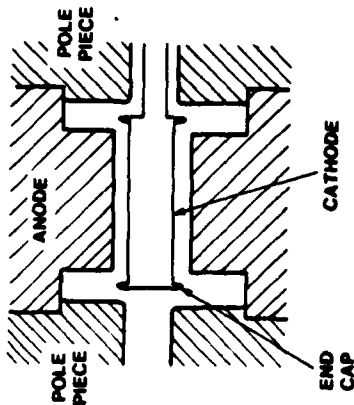


Figure 20 Plots of $\ln(I)$ vs X^* . (a) 0.15 cm gap data of Fig. 7(a)
(b) 0.3 cm gap data of Fig. 7(b)



(b) MARCONI CW-10 MAGNETRON (HARVEY)

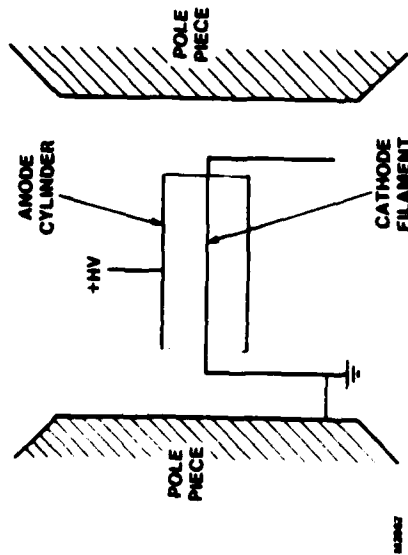


Figure 21 Configuration of Previous Magnetron Experiments (a) Geometry of AD9-6E Magnetron (Jepsen et. al.), (b) Geometry of Marconi CW-10 Magnetron (Harvey et. al.)

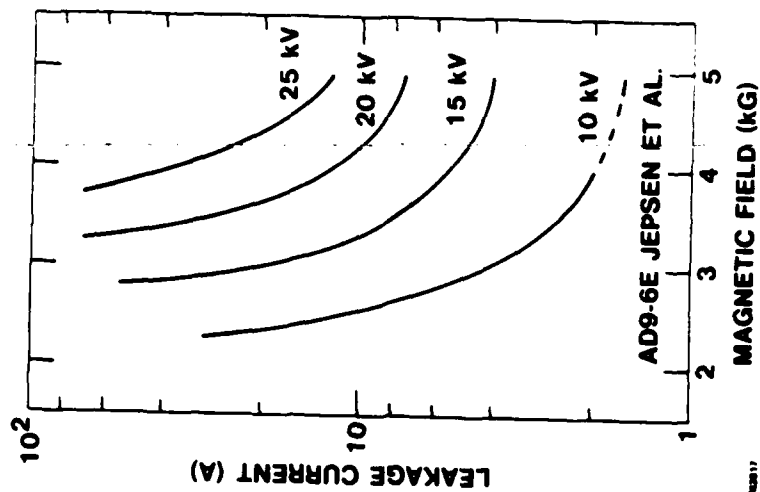


Figure 22 Magnetron Leakage Current vs Magnetic Field Strength (replotted from Fig. 3 of Jepsen et. al.)

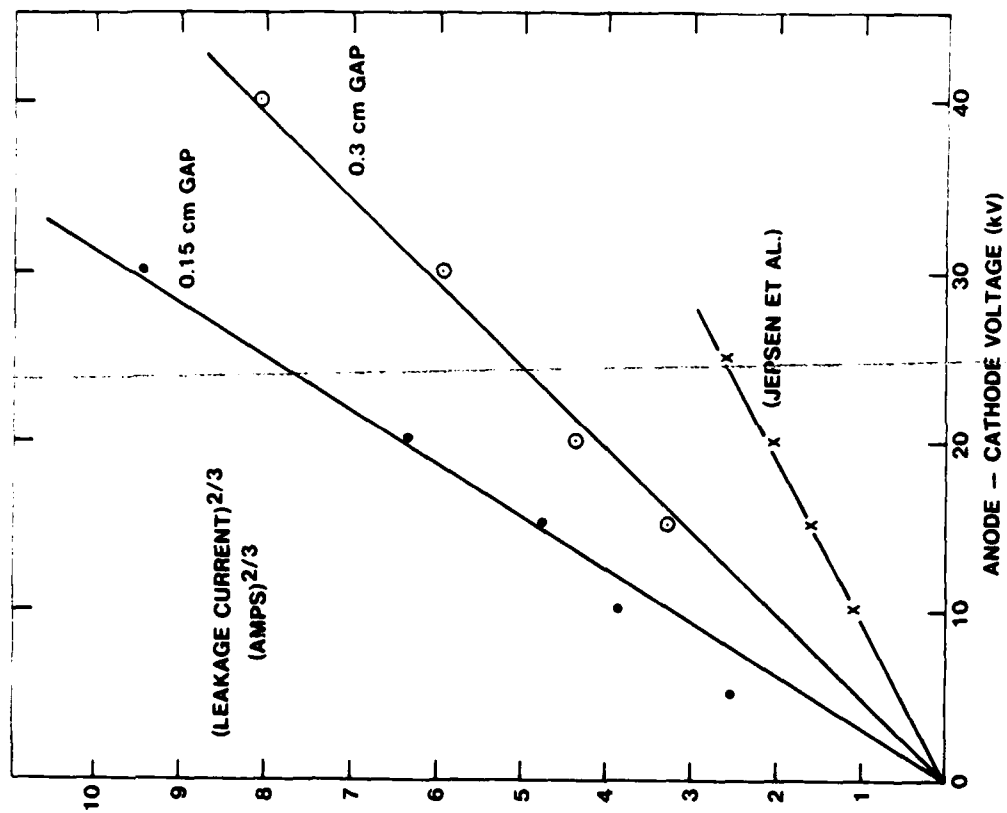


Figure 24 $X^* \rightarrow 0$ Intercept Current to the $2/3$ Power vs A-K Voltage for Present Experiment and Experiment of Jepsen et. al.

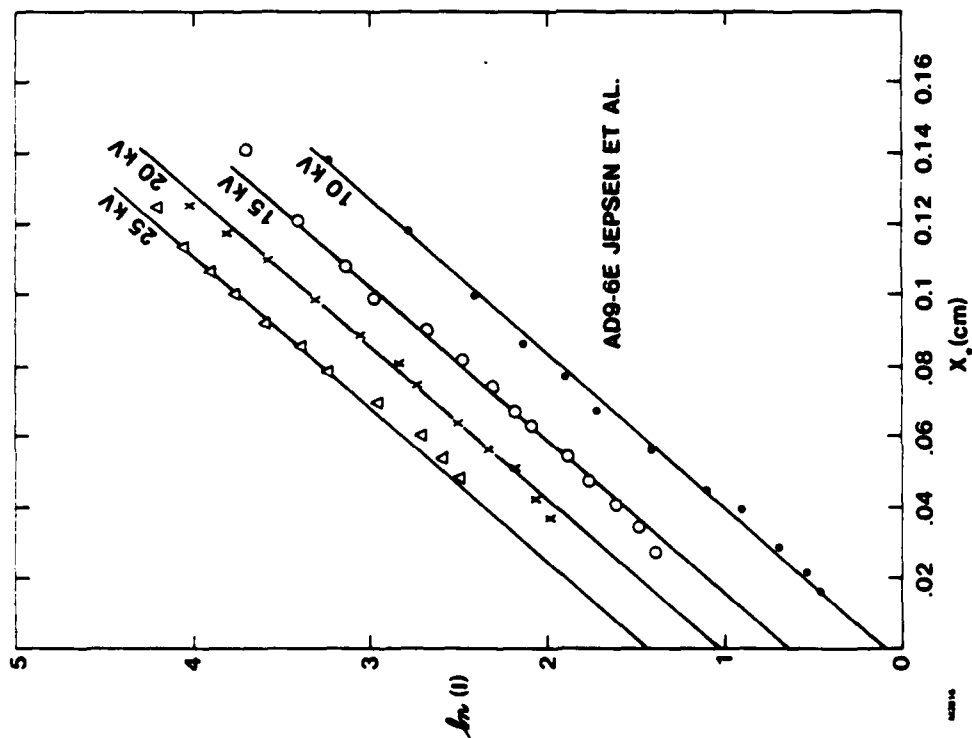


Figure 23 Plots of $\ln(I)$ vs X^* for AD9-66E Data of Fig. 22

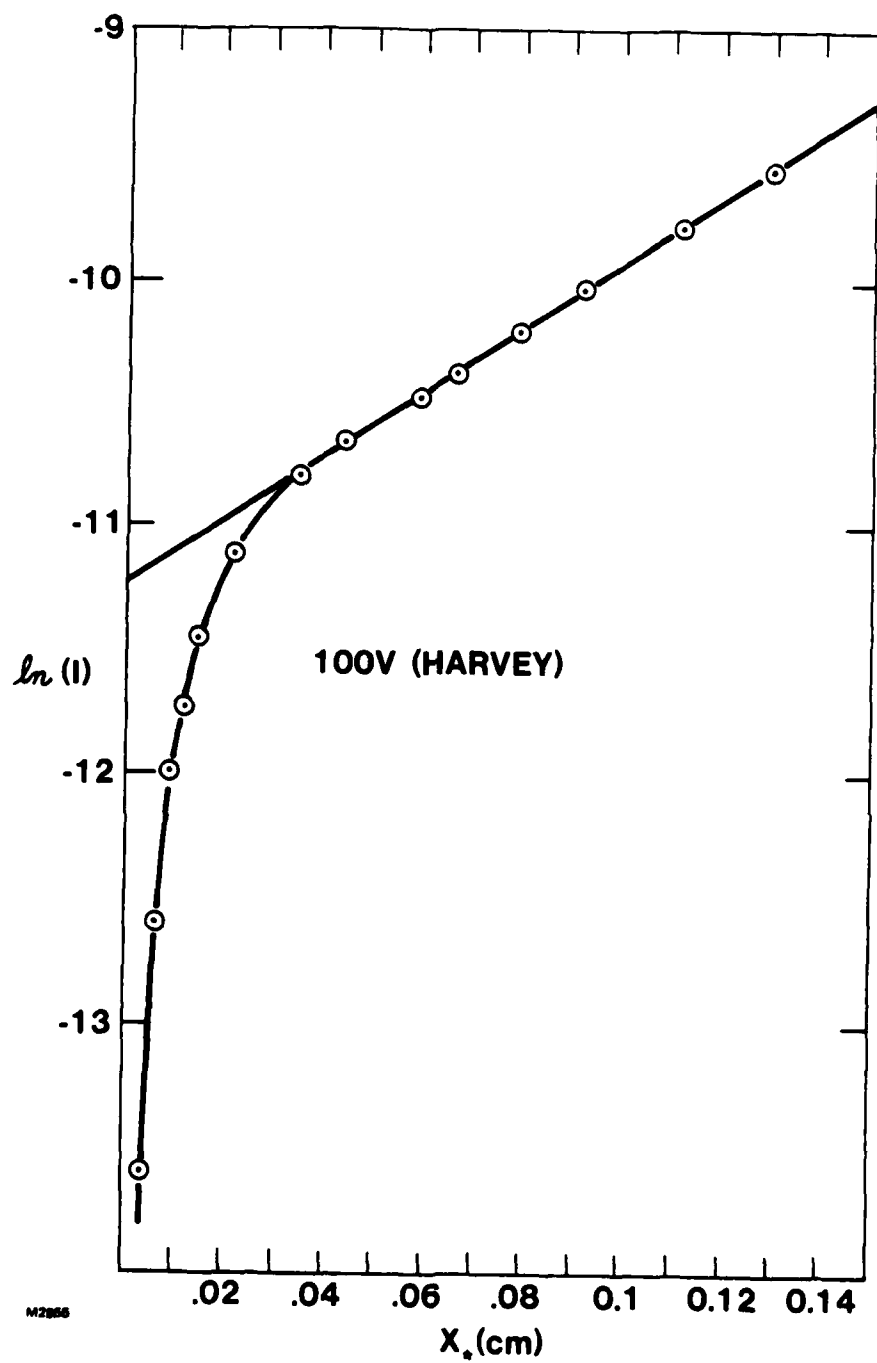


Figure 25 $\ln(I)$ vs x^* for Marconi CW-10 Magnetron Data at 100 V.

ated smooth-anode magnetron which was geometrically very different from the present structure in that its cathode was a heated filament of radius 77 times less than the anode (Figure 21(b)). At low x_* there is a pronounced reduction in anode-cathode leakage similar to that observed in the present experiment (Figure 20(a)). We believe this could be due to a critical value of x_*/d below which there is no synchronous stream in the electron layer, hence no instability. This is substantiated by similar sharp decreases in wave amplitude (Figure 19) at low values of x_*/d .

Although the quantitative similarities between the three sets of data are not so immediately obvious, it is possible to represent all the data (in the linear regime) by a single formula with only a geometrical factor ranging between 1 and 3 to make the change from $r_a \sim r_c$ to $r_c/r_a \ll 1$. In Table 1 be note that the cathode area, rather than the anode area, can be used to reduce the numerical coefficient of the leakage formulae to within a factor of 3 across the four data sets. In the Jepsen data the cathode end caps only extend half the distance to the anode, and electrons flowing past the outer edge of the caps are able to follow magnetic field lines to the pole pieces which are at anode potential. We therefore suppose that the diffusion denominator, d_{eff} , for this device should be computed as if for an anode radius equal to the cap outer radius, but we calculate x_* from d_{eff} relating to the full anode radius. In the Harvey experiment there are no end barriers, but electron confinement is obtained because the magnet pole pieces are maintained at the cathode potential. The common formula for the leakage current in the linear regime of $\ln(I)$ vs x_* is (MKS)

$$I = \frac{0.84 \times 10^{-6} \xi A_c V^{3/2}}{d_{\text{eff}}} \exp \left\{ \frac{4015 x_*}{\xi} \right\} \text{ Amps} \quad (11)$$

- A_c = Area of cathode
- d_{eff} = $(r_a^2 - r_c^2)/2r_a$
- r_a = anode radius
- r_c = cathode radius
- V = anode-cathode voltage

TABLE 1
EXPERIMENTAL DATA

Experiment	Cathode Radius r_c (m)	Anode Radius r_a (m)	Cathode Length l_c (m)	Cathode Area A_c (m ²)	Effective Gap d_{eff} (m)	Leakage Perveance, Slope of $\ln I$ $x_* = 0$ Intercept (Amp)(Volt) ^{-3/2}	C_1 (m ⁻¹)	Linear Region Coefficient C_0
present, 0.15 cm gap	2.54×10^{-2}	2.69×10^{-2}	6.3×10^{-2}	1.00×10^{-2}	0.147×10^{-2}	5.77×10^{-6}	4070	8.44×10^{-7}
present, 0.3 cm gap	2.54×10^{-2}	2.84×10^{-2}	6.3×10^{-2}	1.00×10^{-2}	0.284×10^{-2}	2.94×10^{-6}	3960	8.30×10^{-7}
Jepsen et. al. Ref. (15)	0.333×10^{-2}	0.526×10^{-2} (CAP) 0.429×10^{-2}	2.3×10^{-2}	4.81×10^{-4}	0.085×10^{-2} (USING CAP RADIUS)	1.07×10^{-6}	2300	1.89×10^{-6}
Harvey Ref. (16)	6.49×10^{-5}	0.50×10^{-2}	3.0×10^{-2} (Approx.)	1.22×10^{-5}	0.25×10^{-2}	1.33×10^{-8}	1280	2.12×10^{-6}

$$\begin{aligned}
 x_{\star} &= (r_{\star} - r_c) = \text{radial extent of electron cloud} \\
 \xi &= \text{geometrical factor} \quad \left\{ \begin{array}{l} \xi = 1.0 \text{ for present experiments} \\ \xi = 2 \text{ for Jepsen et al. data} \\ \xi = 3.14 \text{ for Harvey data} \end{array} \right.
 \end{aligned}$$

If the wave amplitude data (Figure 19) is compared with the leakage data (Figure 20) striking similarities are observed. In particular, at fixed x_{\star} the amplitude has an exact $V^{3/2}$ dependence. At $x_{\star}/d > 0.02$ the curves tend to straight lines of slope $\sim 5 \times 10^3 \text{ m}^{-1}$. If reduced to a direct dependence on x_{\star} this agrees within a factor of 1.2 with the slope of the leakage current vs x_{\star} discussed above. Finally, at very small x_{\star} the wave amplitude decreases steeply indicating stabilization of the waves.

7.0 SUMMARY AND CONCLUSION

We have experimentally investigated the flow and stability of electrons in a crossed electric and magnetic field. Unstable transverse magnetic waves were observed at frequencies predominantly below the electron cyclotron frequency with wavelengths much greater than the electron layer thickness. The phase velocity of the waves was approximately equal to the $E \times B$ velocity of the electrons at the surface of the electron layer.

The waves are believed to be driven unstable by a resistive wall instability. When the thickness of the electron layer is reduced the influence of the resistive anode appears to decrease thus lowering the wave amplitude. At very small x_*/d , strong stabilization is observed.

The electron leakage current was found to obey an analytic relation which is in close agreement with previous experiments. We believe the source of the leakage current is unstable TM waves causing a drift of electrons towards the anode. This fact is supported by the strong correlation between the wave amplitude and leakage current data.

More theoretical work is required to explain why the magnetron instability, which has a higher theoretical growth rate than the resistive wall instability, was not observed in this experiment or previous experiments.⁴ In addition, further experimental work on the electron distribution^{18,19} in the A-K gap would be useful for future theoretical analysis.

Acknowledgments

It is a pleasure to acknowledge the experimental assistance of James Gardner and stimulating discussion with Richard Patrick and G. Sargent Janes of this Laboratory. The work was supported jointly by ARO, ONR and AFOSR via contract DAAG29-84-C-0007.

REFERENCES

1. M.S. DiCapua, and D.G. Pelliman, J. Appl. Phys. 50, 3713 (1979).
2. S. Humphries, Bull. Am. Phys. Soc. 18, 1310 (1973).
3. Y. Carmel, and J. Nation, Phys, Rev. Lett. 31, 286 (1973).
4. T.J. Orzechowski, and G. Bekefi, Phys. Fluids 19, 43 (1976).
5. J. Eninger, APS Bulletin 29, 1342 (1984).
6. O. Buneman, J. Electron 3, 1 (1957).
7. G.G. MacFarlane, and H.G. Hay, Proc. Phys. Soc., (London) Sec. B63, 409 (1949).
8. R.H. Levy. Phys. Fluids 8, 1288 (1965).
9. J. Swegle, and E. Ott, Phys, Rev. Lett. 46, 929 (1981).
10. J. Swegle, and E. Ott, Phys. Rev. Lett. 24, 1821 (1981).
11. D.P. Chernin, Phys, Fluids 25, 1342 (1982).
12. J. Swegle, Phys. Fluids 26, 1670 (1983).
13. C.L. Chang et. al., Phys. Fluids 27, 2545 (1984).
14. R.V. Lovelace, and E. Ott, Phys. Fluids 17, 1263 (1974).
15. E. Ott, and R.V. Lovelace, Appl. Phys. Lett 27, 378 (1975).
16. R.L. Jepsen and M.W. Muller, J. Appl. Phys. 22, 1196 (1951).
17. H.F. Harvey, "High Frequency Thermionic Tubes," Ch 4 (John Wiley and Sons, Inc., New York, 1943).
18. L.E.S. Mathias, J. Electr. Contr. 1, 8 (1955).
19. H.C. Nedderman, J. Appl. Phys, 26, 1420 (1955).

END

5-87

DTIC